

Decoding of Context-Dependent Olfactory Behavior in *Drosophila*

Highlights

- Olfactory behavior is predicted by superposition of normalized glomerular activity
- Behavioral/neuronal responses to binary mixtures scale linearly with mixing ratio
- Manipulation of glomerular activity biases behavior according to the decoding model
- Relative valence of odors changes and even switches depending on the context

Authors

Laurent Badel, Kazumi Ohta,
Yoshiko Tsuchimoto, Hokto Kazama

Correspondence

hokto_kazama@brain.riken.jp

In Brief

Badel et al. show that flies' innate odor responses can be predicted by a weighted sum of normalized glomerular activity. They further demonstrate that relative odor preference switches depending on the olfactory context as predicted by their decoding model.

Decoding of Context-Dependent Olfactory Behavior in *Drosophila*

Laurent Badel,¹ Kazumi Ohta,¹ Yoshiko Tsuchimoto,¹ and Hokto Kazama^{1,*}

¹RIKEN Brain Science Institute, 2-1 Hirosawa, Wako, Saitama, 351-0198, Japan

*Correspondence: hokto_kazama@brain.riken.jp

<http://dx.doi.org/10.1016/j.neuron.2016.05.022>

SUMMARY

Odor information is encoded in the activity of a population of glomeruli in the primary olfactory center. However, how this information is decoded in the brain remains elusive. Here, we address this question in *Drosophila* by combining neuronal imaging and tracking of innate behavioral responses. We find that the behavior is accurately predicted by a model summing normalized glomerular responses, in which each glomerulus contributes a specific, small amount to odor preference. This model is further supported by targeted manipulations of glomerular input, which biased the behavior. Additionally, we observe that relative odor preference changes and can even switch depending on the context, an effect correctly predicted by our normalization model. Our results indicate that olfactory information is decoded from the pooled activity of a glomerular repertoire and demonstrate the ability of the olfactory system to adapt to the statistics of its environment.

INTRODUCTION

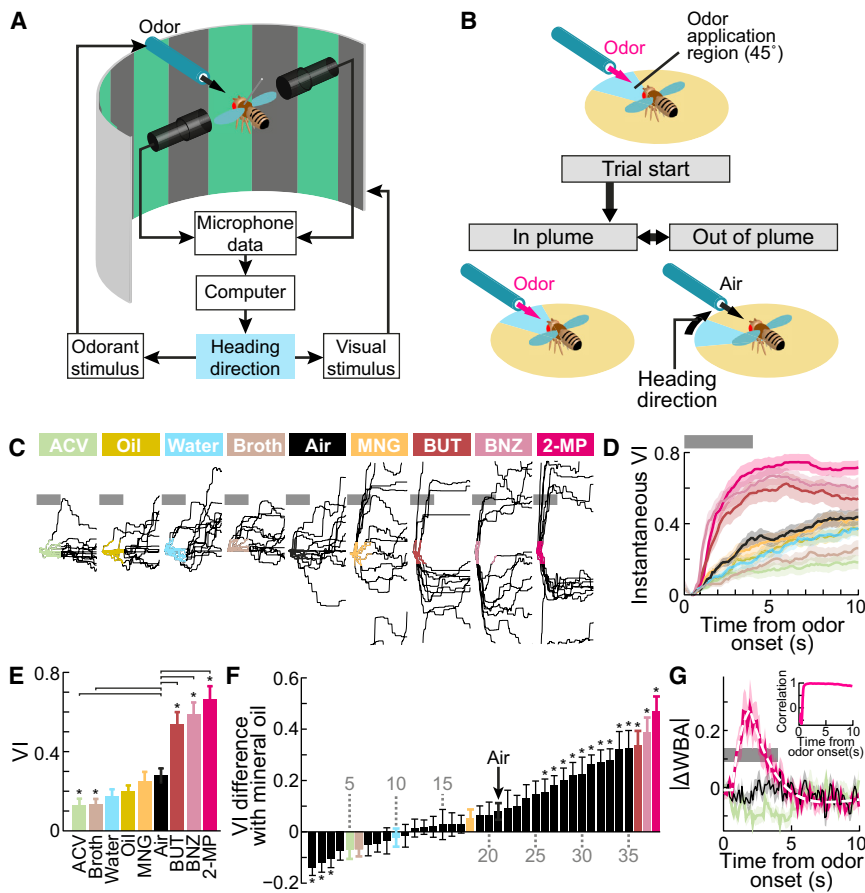
A prominent feature of the olfactory system is its widely distributed code. Even monomolecular odorants typically bind to multiple types of olfactory receptors (Malnic et al., 1999), recruiting multiple postsynaptic glomeruli without apparent spatial or chemotopic organization. Different odorants recruit different sets of glomeruli (Friedrich and Korsching, 1997; Hallem and Carlson, 2006; Joerges et al., 1997; Ng et al., 2002; Rubin and Katz, 1999; Uchida et al., 2000; Wang et al., 2003) with distinct temporal dynamics (Cury and Uchida, 2010; Friedrich and Laurent, 2001; Spors and Grinvald, 2002; Wehr and Laurent, 1996), and most glomeruli respond to a wide array of odors. These observations demonstrate that in a range of organisms, including insects, fish, and mammals, early olfactory information is represented as spatio-temporal patterns of glomerular activity. How these activity patterns are decoded by the brain to guide odor-evoked behavior, however, remains largely unknown.

Olfactory research in *Drosophila melanogaster* has provided elements of answer to this question. Using behavioral genetics, attraction, and aversion to specific odors have been linked to the activation of one or a few glomeruli in the antennal lobe

(AL) (Ai et al., 2010; Dweck et al., 2013; Min et al., 2013; Ronderos et al., 2014; Schlief and Wilson, 2007; Semmelhack and Wang, 2009; Stensmyr et al., 2012; Suh et al., 2004). These observations suggest a labeled-line coding strategy, in which individual glomeruli convey signals of specific ethological relevance for the animal and their activation triggers the execution of hard-wired behavioral programs. However, it remains uncertain whether this is a property of a specialized subset of glomeruli or constitutes a general coding principle in the AL. More importantly, how compound signals from multiple glomeruli are integrated to determine the valence of odors, including mixtures of odors commonly found in natural environments, is poorly understood (Kreher et al., 2008).

Another open question is the coding beyond absolute odor valence. Flies, for example, choose the less aversive odor when forced to make a choice between two inherently aversive stimuli (Tully and Quinn, 1985). Moreover, studies in humans have shown that the evaluation of relative odor valence changes depending on the context (Clepece et al., 2014). How relative valence is computed in the brain and how it is modulated according to the context remains elusive, although a recent study showed that divisive normalization can explain context-dependent choice behavior in primates (Louie et al., 2013).

Here, we used a combination of optical imaging and behavioral techniques to address these questions systematically. We used two-photon imaging to monitor Ca^{2+} signals in the whole AL in response to a diverse set of odors. Comparing these data with odor-evoked behavioral responses allowed us to formulate a decoding model describing how innate olfactory behavior is dictated by the population of projection neurons (PNs), the AL output neurons, in a quantitative manner. We found that a weighted sum of normalized PN responses can recapitulate observed behavior and predict responses to novel odors, including mixtures and odors at different concentrations. The valence assigned to individual glomeruli in our analysis is consistent with previous findings; however, the contribution of individual glomeruli to the behavioral output is small, indicating that odor valence is not dominated by a few privileged glomeruli but depends on pooling small contributions over a large number of glomeruli. This conclusion is further supported by genetic silencing and optogenetic activation of individual olfactory receptor neuron (ORN) types, which evoked modest biases in behavior in accordance with the model predictions. Strikingly, behavioral responses were altered when the same odors were tested in different olfactory contexts. Our decoding model captured this adaptive behavior and correctly predicted that the relative preference of pairs of odors could switch depending



(F) Mean VI values for 36 pure odorants and 3 control stimuli ($n = 20\text{--}23$ flies for each stimulus), relative to mineral oil, in increasing order. Error bars indicate SEM. Asterisks denote stimuli significantly more attractive (3) or aversive (13) than mineral oil (Wilcoxon signed-rank test, Bonferroni-corrected, $p < 0.05$). Colored stimuli are common with (C)–(E); identity of other stimuli is listed in Table S1.

(G) Absolute difference in left and right wing beat amplitudes (mean over all trials and flies) against time from odor onset, for the most attractive (green, ACV) and the most aversive (magenta, 2-MP) odors in (E) and air (black). Aversive response is fitted with a sum of exponentials (dashed line). Shaded regions denote SEM over flies ($n = 20$). Inset: Pearson correlation between the VI and cumulative $|\Delta WBA|$, for odor set in (E).

on the olfactory context. These results highlight the ability of the olfactory system to adapt to the statistics of its olfactory environment, similarly to the visual and auditory systems (Kohn, 2007; Wark et al., 2007).

RESULTS

Differential Responses to Attractive and Aversive Odors in a Flight Arena

We first sought to characterize odor-evoked behavioral responses by monitoring the behavior of tethered flies in a flight-simulator arena. The arena was equipped with a closed-loop feedback system that allowed animals to virtually adjust their heading direction by modulating the amplitudes of their left and right wing beats (Figures 1A and S1). A change in heading direction was accompanied by a corresponding rotation of the visual and olfactory landscapes, defining a virtual-reality-like environment for the animal to navigate. Olfactory stimuli were delivered in the form of a plume, spanning 45° in azimuth, which

flies were free to exit or re-enter by adjusting their heading direction (Figure 1B). The valence of olfactory stimuli in this setup could thus be assessed by monitoring the tendency to navigate in or out of the odor plume.

We initially characterized odor-evoked behavior in this assay using a set of six odorants, which we expected on the basis of prior reports (Knaden et al., 2012; Semmelhack and Wang, 2009) and preliminary experiments to be either strongly attractive or aversive, and three control stimuli (mineral oil, water, and air). Flies often exited aversive odors by producing a fast saccadic turn (Figure 1C). Similar avoidance behavior was not observed in response to air, for which trajectories only showed occasional low-amplitude saccades. Attractive odors, on the other hand, evoked a reduction in turning rate and a tendency to navigate in the odor for a longer time.

To quantify these responses, we defined a measure of olfactory preference termed valence index (VI) as the proportion of time spent outside the odor plume. When computed relative to the time of odor application, instantaneous VIs increased

Figure 1. Differential Responses to Attractive and Aversive Odors in a Flight Arena

(A) Schematic of the virtual-flight arena. Flight behavior is probed using microphones, whose output is fed to a closed-loop feedback system that updates visual and olfactory stimuli in real time.

(B) Schematic of the behavioral assay. The fly starts each trial in the center of the odor plume,

after which it is free to adjust its heading direction to navigate in or out of the plume.

(C) Trajectories of a representative fly's orientation in the flight simulator in response to 15 repeated applications of six odors and three control stimuli (mineral oil, water, and air). Gray bar indicates the period of odor delivery (4 s). Colored portions indicate that the animal is navigating in the plume. Attractive odors (leftmost) evoke little turning responses in contrast with aversive odors (rightmost), for which sharp turns are observed in the majority of trials. ACV, apple cider vinegar; MNG, mango mimic; BUT, butanal; BNZ, benzaldehyde; 2-MP, 2-methylphenol.

(D) Instantaneous value of the valence index (VI, the proportion of time spent outside the odor plume) plotted relative to the onset of odor application for the nine stimuli in (C). Shaded regions denote SEM computed over flies ($n = 20$). VI values are best separated near the end of the odor application period (horizontal gray bar).

(E) Mean VI values computed by averaging the instantaneous VI in the last 1 s of odor application. Error bars indicate SEM over tested flies ($n = 20$). Asterisks denote statistically significant differences compared with the air control in black (Wilcoxon signed-rank test, Bonferroni-corrected, $p < 0.05$). Mineral oil and water evoke mildly attractive responses compared to air.

monotonically and showed consistent trends extending beyond the period of odor application (Figure 1D). Given that attractive and aversive VIs were best separated near the end of the odor application period, we scored each odor using the mean VI value in the last 1 s of odor application (Figure 1E; our results are largely independent of the choice of the scoring period, see Figure S1).

Of the six tested odors, two attractive and three aversive odors evoked significant responses compared with air (Figure 1E). Solvents also evoked mildly attractive responses. Attraction to humidified air has been documented and is strongly reduced by the mutation of Orco (Lin et al., 2015). Attraction to mineral oil also likely depends on the olfactory system, as mineral oil evoked sparse but significant glomerular activity in our measurements (see Figure 2D), and blocking synaptic transmission in Orco-dependent ORNs evoked a small increase in VI (Figure S2).

To further examine responses to diverse odors, we screened odor-evoked responses to a panel of 84 odors, consisting of 36 pure odorants, 4 of which were sampled at 4 different concentrations, and 36 binary mixtures of attractive and aversive odors at various ratios (Table S1). Odors were sampled in sets of 6 and delivered sequentially in each experiment. To verify that the baseline behavior was consistent across different odor sets, we included mineral oil in every experiment. VI values for the 36 pure odorants showed a nearly continuous array of responses (Figure 1F). After correcting for multiple comparisons, 3 odorants were significantly more attractive, and 13 were more aversive, than mineral oil. When compared to air, odors were almost symmetrically split into two sides (Figure 1F). These results demonstrate that flies exhibit both attraction and aversion in response to a variety of odors in our assay.

Fast Escape Responses to Aversive Olfactory Stimuli

Inspection of individual flight trajectories (Figure 1C) revealed that escape responses to aversive stimuli can be remarkably fast. Because flight orientation is controlled by the relative amplitude of wing beats, we computed the absolute difference between the left and the right wing-beat amplitudes (Δ WBA). As expected, air did not evoke noticeable changes in Δ WBA (Figure 1G). In contrast, aversive odors evoked a sharp, transient increase in Δ WBA, whereas attractive odors evoked a slower, sustained decrease. VI values were tightly correlated with the cumulative Δ WBA (Figure 1G, inset), confirming that our behavioral measure reflects an active, stimulus-evoked modulation of the turning rate.

To estimate the response latency, we fitted Δ WBA for an aversive odor with a sum of exponentials (Figure 1G). The fitted curve deflected (10% rise time) 200 ms after the first contact with the odor, indicating that the time required to perceive, process, and respond to an aversive stimulus is shorter than 200 ms.

In Vivo Ca^{2+} Imaging of PN Responses in 37 Identified Glomeruli

We next examined PN activity in response to the same panel of odors under identical odor delivery conditions. In the fly AL, inputs from ORNs are segregated into ~50 glomeruli, all of which are identifiable across individuals (Couto et al., 2005; Fishilevich

and Vosshall, 2005; Vosshall et al., 2000). Because PNs in the same glomerulus transmit highly correlated information (Kazama and Wilson, 2009), each glomerulus can be considered as a unit of output. Therefore, the entire olfactory information transmitted from the AL can be obtained by monitoring PN activity in a mere ~50 dimensional space. To achieve this, we expressed the calcium sensor GCaMP6f (Chen et al., 2013) under the control of NP225-Gal4 (Tanaka et al., 2012; Thum et al., 2007), which labels 37 glomeruli with high specificity (Figure 2A). GCaMP fluorescence in the entire AL was imaged at ~1.7 Hz using two-photon microscopy in response to the 84 odors in our dataset. To account for brain movement during recordings and variability in AL morphology across animals, we registered all images to a template AL (Figure 2B), and the fluorescence in each glomerulus was extracted by averaging over the spatial extent of the corresponding glomerulus in the template (Figure S3). Consistent with previous reports, glomeruli exhibited various tuning breadths: a glomerulus responded on average to $22\% \pm 16\%$ (mean \pm SD) of all tested odors. Similarly, odors recruited on average 8 ± 5 of the 37 glomeruli (Figures 2C and 2D).

Odor Onset Responses Carry Enough Information to Classify Odors

The rapidity of aversive responses suggests that animals rely on the instantaneous, spatial dimension of PN responses to make perceptual decisions. This requires that a single “snapshot” of the PN response contain sufficient information to categorize odorants. To verify this, we trained a linear classifier to predict odor identity based on PN responses in a single imaging frame. Because each odor was presented four times in each animal, we used data from three trials to train the classifier and the remaining trial to test classification performance. As expected, classification accuracy was close to chance level before odor application, and increased shortly after odor onset (~150 ms after odor contact; Figure 2E), peaking near 65% over time (~1.3–3.7 s after odor contact). It is worth noting that the onset of this increase in classification accuracy matches well with the onset of the aversive response. Performance decayed after odor offset; however, it remained well above chance level throughout the recording period (13 s beyond odor offset), suggesting that residual PN responses carry a significant amount of information about past stimuli.

Responses to Binary Mixtures Suggest Linear Integration of Olfactory Channels

Comparing behavioral and imaging data showed that PN responses in a number of glomeruli exhibited significant linear correlations with VI (Figure S4), suggesting some degree of linearity in the transformation from PN responses to behavior. The total AL activity, however, only correlated weakly with behavior (Figure S4), indicating that the intensity of AL activation is not the sole determinant of odor valence. To examine the relationship in more detail, we focused on mixture data and asked whether behavioral and physiological responses vary in proportion to the mixing ratio of the components. VI scaled linearly with the mixing ratio (Figure 3A). This trend was paralleled in PN activity: linearly regressing the vectors of PN responses on the mixing ratio lead to a very accurate description of PN data (R^2 of fit

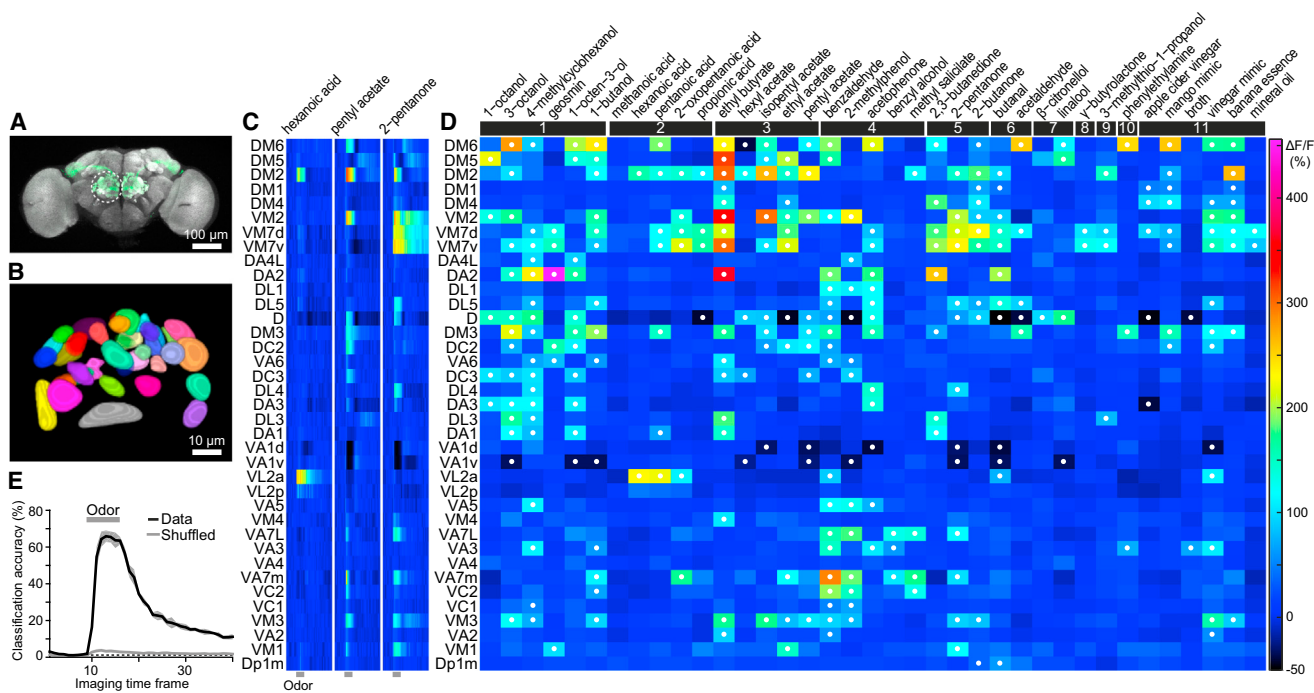


Figure 2. Odor Representations in the Antennal Lobe PNs

(A) Expression pattern of *NP225-Ga4* in the adult brain (*NP225-Ga4/UAS-mCD8::GFP*). The brain was stained with nc82 (gray) and anti-GFP (green). White circle indicates the region scanned in imaging experiments (right antennal lobe).

(B) Template antennal lobe used in image registration, showing the spatial arrangement of 37 glomeruli labeled by *NP225-Ga4* (arbitrary color code).

(C) Sample Ca^{2+} responses to three odors. $\Delta F/F$ of GCaMP6f fluorescence is color coded according to the scale bar in (D). Horizontal axis is time (40–595 ms frames), vertical axis is glomerulus. Gray solid bar at the bottom indicates the period of odor application (4 s).

(D) Mean Ca^{2+} responses to 36 pure odors and the mineral oil solvent (imaging frames 10–17, $n = 4$ –9 brains). Odors are arranged by functional groups: 1, alcohols; 2, acids; 3, esters; 4, aromatics; 5, ketones; 6, aldehydes; 7, terpenes; 8, lactones; 9, sulfur compounds; 10, amines; 11, multimolecular compounds. Significant responses are marked with a white dot (Mann-Whitney U test, $p < 0.01$, see [Supplemental Experimental Procedures](#)).

(E) Odor classification performance as a function of imaging time frame. The task was to classify 84 odors given the response of 37 glomeruli in a single imaging frame. Shaded region shows SD over four classifiers, each of which uses a different imaging trial as the test. Gray line shows performance after shuffling glomerulus labels. Dotted line indicates chance level (1/84).

0.6–0.97; [Figure 3B](#)). These results suggest a linear relationship between PN responses and behavior.

Olfactory Contrast Normalization Enables Accurate Decoding of PN Responses

Linear models are widely used to examine the relationships between neuronal activity and behavior. In larval *Drosophila*, a linear model based on the activity of ORNs was successful in predicting behavioral responses to a panel of 26 odorants ([Kreher et al., 2008](#)). To test whether this framework could explain our data quantitatively, we constructed a decoding model (referred to as linear model) in which the VI is calculated as a weighted sum of glomerular activity ([Figure 4A](#)). We fit the model parameters using regularized linear regression (see [Experimental Procedures](#)) with training data, and examined its predictive power with test data not used in the fitting procedure. Prediction performance was evaluated using the R^2 coefficient (see [Experimental Procedures](#)). Unexpectedly, we found that while the model could accurately describe the training data, it performed poorly at predicting the test data ([Figure 4B](#)).

We reasoned that a possible cause for the failure of the linear model is that odorants were delivered in sets of six in our experiments: the response to one of the odors in the set may be affected by the experience of the other five odors, for example, through sensory adaptation. To test this, we constructed a second decoding model (referred to as normalization model) in which glomerular outputs were passed through a nonlinear normalization step before the summation ([Figure 4A](#)). Normalization is meant to represent adaptation to the statistics of the olfactory environment and was minimally modeled using a mean subtraction followed by a rescaling by the SD of each glomerulus' response to the odor set, both of which commonly describe neuronal adaptation ([Baccus and Meister, 2002](#); [Chandrasekaran and Chichilinsky, 2001](#); [Nagel and Doupe, 2006](#); [Ohzawa et al., 1985](#)). Importantly, this form of normalization is compatible with the linearity observed in response to mixtures.

We fit the model parameters using the same procedure as for the linear model. Notably, we found that the normalization model not only accurately described the training data, but also yielded accurate predictions of the test data ([Figure 4B](#)). This prediction performance was highly significant (permutation test, $p < 0.002$),

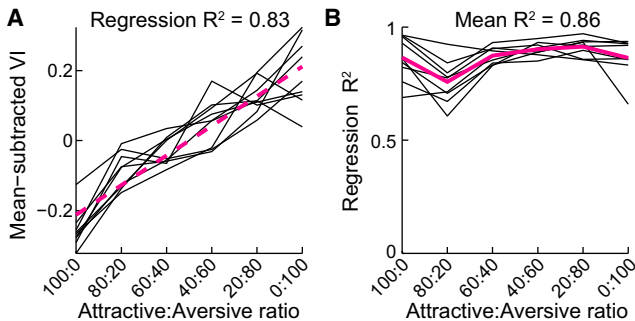


Figure 3. Linearity of Neuronal and Behavioral Responses to Binary Mixtures of Attractive and Aversive Odors

(A) VI (mean subtracted) in response to mixtures of increasingly aversive content, for nine different binary mixture sets ($n = 20\text{--}27$ flies for each mixture) of three attractive and three aversive odors (Table S1). Magenta dashed line is a linear fit to the data.

(B) Linearity of PN responses assessed by fitting the six 37-dimensional vectors of PN responses to each binary mixture set using linear regression. The R^2 coefficient is shown as a function of mixing ratio for each of the nine mixture sets (black lines). Magenta line is the average R^2 over the nine mixtures. Mean R^2 across mixture ratios is 0.86.

suggesting that the normalization operation renders the relationship between the predictors (glomerular activation) and the dependent variable (VI) more linear.

We next tested how the performance varied with the number of glomeruli included in the list of predictors. Because sampling all possible subsets of 37 glomeruli would be computationally prohibitive, we tested instead a multitude (742,700) of randomly chosen subsets. The average prediction performance increased monotonically with the number of glomeruli (Figure 4C, top graph). Importantly, even when restricted to only the best subset of each size (Figure 4C, bottom graph; see *Supplemental Experimental Procedures* for definition of best subsets), the performance continuously increased up to intermediate sizes (~ 20 glomeruli) before slight overfitting occurred. These results suggest that the majority of glomeruli carry information about the dependent variable.

A final model was constructed by averaging the sets of glomerulus weights obtained in the cross-validation procedure. This resulted in a balanced number of 18 attractive and 19 aversive glomeruli (Figure 4D). We confirmed that the model accurately explained the responses to pure odors and mixtures (Figure 4E), and further challenged the model with an additional set of test data consisting of four odors at three different concentrations. Again, while the linear model failed to predict these data quantitatively, the normalization model gave accurate predictions (Figure 4E).

Silencing Subsets of Olfactory Receptor Neurons Weakly Biases Behavioral Output

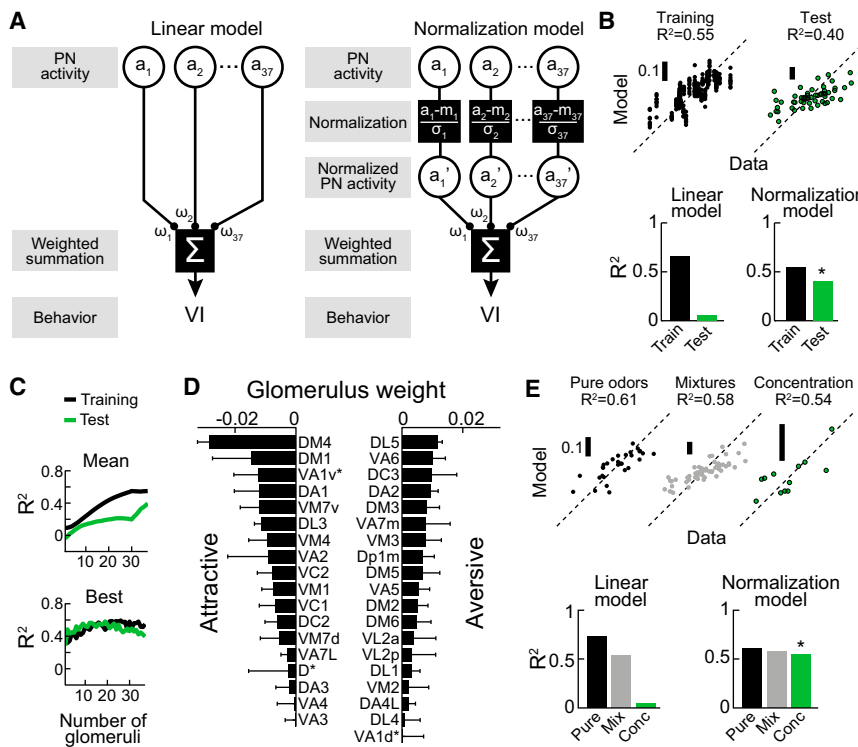
These results demonstrate strong correlation, but not causality, between glomerular response and behavioral output. To test the causal relationship, it is necessary to perturb glomerular activity and assess the impact of the manipulation on the behavior. To achieve this in a highly glomerulus-specific manner, we genetically silenced synaptic input to glomeruli by expressing tetanus toxin

(TNT), a potent blocker of vesicular release (Sweeney et al., 1995), in ORNs using Or-Gal4 drivers, which drive virtually no expression outside the target ORNs (Couto et al., 2005; Fishilevich and Vosshall, 2005). We targeted five different glomeruli: DM1, DM4, DM5, DC3, and VC1. These particular glomeruli were chosen in part on the basis of their established attractive or aversive role, and partly based on the predictions of our model. In an attempt to evoke larger effects, we tested two lines in which TNT was co-expressed in three different ORN types. A first set (glomerulus DM5, DC3, and VC1) was chosen to evoke changes toward more attractive VI values and a second set (glomerulus DM4, VA2, and VA4) was selected to induce more aversive responses.

A number of results supported the conclusion that behavior is determined by the summed activity of many glomeruli. First, in accordance with the prediction that blocking input to a small number of glomeruli should have limited behavioral effect, VIs in flies expressing TNT in one or three glomeruli were not substantially different from those in the control flies (Figure 5A). Notably, blockade of synaptic transmission in DM1 or DM5 ORNs, which abolished attraction or aversion to different concentrations of apple cider vinegar in walking flies (Semmelhack and Wang, 2009), did not remove innate responses to this as well as other odors in our experiments (Figure 5A). To rule out the possibility of an incomplete effect of TNT, we expressed TNT in either DM1 or DM5 ORNs while expressing GCaMP3 (Tian et al., 2009) in PNs under the control of GH146-QF (Potter et al., 2010) and quantified the change in postsynaptic PN responses to ethyl acetate, an odor that activates both types of ORNs. PN activity in glomerulus DM5 was completely abolished when TNT was expressed in presynaptic ORNs (Figure 5B). Thus, the limited behavioral effect of ORN blockade cannot be attributed to an incomplete action of TNT at least in the case of DM5. In glomerulus DM1, the reduction in PN response was only $\sim 40\%$ (Figure 5B); however, this residual activity is likely to be the result of lateral interactions between glomeruli, which provide excitatory drive to PNs whose cognate ORNs are silenced (Olsen et al., 2007; Root et al., 2007; Shang et al., 2007). To examine this possibility, we inferred a PN-PN connectivity matrix using the correlation structure of Ca^{2+} signals during the baseline period (Figure S5 and *Experimental Procedures*) and used the resulting connectivity to estimate odor-evoked PN activity in TNT-positive flies. This model accurately predicted both the moderate decrease in DM1 and the strong decrease in DM5 activity in the absence of direct ORN input (Figure 5C). These results support the conclusion that olfactory behavior during flight is not dictated by a few privileged glomeruli.

Second, a closer inspection revealed that VIs were biased in a direction consistent with the weight of each glomerulus in our model. When we computed the correlation between the estimated TNT-induced change in PN activity and the change in VI, the sign of the correlation matched the expected sign in all cases (Figure 5D). Interestingly, synaptic blockade in DM4 and VC1 had an effect on behavior, which was never reported previously, thus expanding the list of contributing glomeruli.

Finally, and most critically, our model quantitatively predicted the behavioral effect of blocking ORNs. We computed the R^2 values between the observed TNT-induced changes in VI and model predictions for single- and triple-ORN blocking



(D) Glomerulus weights in the final model (average over the nine sets of regression weights obtained in cross-validation). Negative weights correspond to attractive and positive weights to aversive glomeruli. Error bars show SD; error bars extending beyond zero have been truncated. Asterisks indicate glomeruli for which the response to more than half of the sampled odors was inhibitory.

(E) Performance of the final model constructed using the weights in (D). Top: scatter plots of the normalization model predictions against measured VI, for the two sets used in cross-validation (pure odors and mixtures) and an additional set of four odors at three concentrations (Table S1). Bottom: a linear model created using the same procedure accurately describes the pure odor and mixture datasets but fails to correctly predict the concentration data. The normalization model yields highly accurate predictions ($p < 0.008$, permutation test). Mix, mixtures; Conc, concentration.

experiments. For both datasets, the R^2 coefficient showed a large increase during the odor-application period (Figure 5E), which was significant (permutation test, $p < 0.006$). The quality of model predictions was higher when three ORN types were manipulated, matching the idea that blocking multiple ORNs evokes larger changes in behavior (Figure 5F). In triple-ORN blocking experiments, performance was maximal when all three glomeruli were blocked in the model, with each individual glomerulus explaining a smaller amount of variance in the data (Figure 5G). This indicates an additive effect of blocking multiple ORN types concurrently. Taken together, these results suggest that blocking ORN biases behavioral output, in a direction determined by the identity of the blocked ORNs, and with amplitude that scales with the change in PN activity in their cognate glomeruli.

Activation of Specific ORNs Evokes Attraction

To further test the causal relationship between glomerular activity and behavior, we asked whether we can bias the behavior according to the model by artificially activating a specific glomerulus. This was achieved by expressing Chrimson, a red-shifted variant of channelrhodopsin (Klapoetke et al., 2014) in ORNs belonging to a particular glomerulus and exciting it with light. We chose to focus on DM4 because this glomerulus had the largest weight in our decoding model. The effectiveness of

Chrimson was verified by recording from antennal ab2 sensilla, which house the DM4 ORNs (ab2A neurons). Application of 637 nm laser light evoked robust increases in firing frequency in ab2A neurons that scaled with light intensity (Figure 6A). We then tested whether light-induced activation of these ORNs had an impact on the behavioral response to odors. We tested two odors, γ -butyrolactone and linalool, which evoke relatively sparse PN activity but excite ab2A neurons. Both odors were significantly more attractive when paired with light than when applied alone (Figure 6B). In contrast, control flies showed no significant change in VI. To further confirm that this increase in attraction is not an artifact of the laser stimulation, we restricted light application to the antennae by covering the eyes and the head cuticle with aluminum foil, so that only the antennae were exposed to the light (Figure 6C). Flies prepared in this way showed a significant decrease in VI in response to light stimulation in the absence of odor (Figure 6C); again, no change was observed in control flies. These results demonstrate that activation of DM4 ORNs evokes attraction in our setup.

Dependence of Relative Valence on the Olfactory Context

One interpretation of the normalization model is that the attractive or aversive effect of a glomerulus is modulated by the

Figure 4. Olfactory Normalization Enables Predictive Decoding of PN Responses

(A) Schematic of the linear and the normalization models. In the normalization model, individual PN responses are normalized, weighted, and summed to produce the estimate of the VI. Normalization parameters (mean, m and standard deviation, σ) are computed using the PN responses to the six odors in each set.

(B) Prediction performance of the linear and the normalization models. Both models are fitted on training data and evaluated on test data using the same procedure. Data comprise 36 pure odors and 36 binary mixtures ($n = 20\text{--}27$ flies for each stimulus). Top: scatter plots of the normalization model predictions against measured VI. Data from nine cross-validation rounds is pooled. Bottom: summary of prediction performance for the two models. Although the linear model accurately describes the training set, it fails to predict the test set accurately. The normalization model yields accurate predictions that were highly significant in a permutation test ($p < 0.002$).

(C) Prediction performance of the normalization model as a function of the number of glomeruli included in the model. 742,700 randomly drawn subsets of glomeruli were sampled and model parameters were fit as in (B). Top graph shows average performance; bottom graph shows performance of the best subset of each size (see *Supplemental Experimental Procedures*).

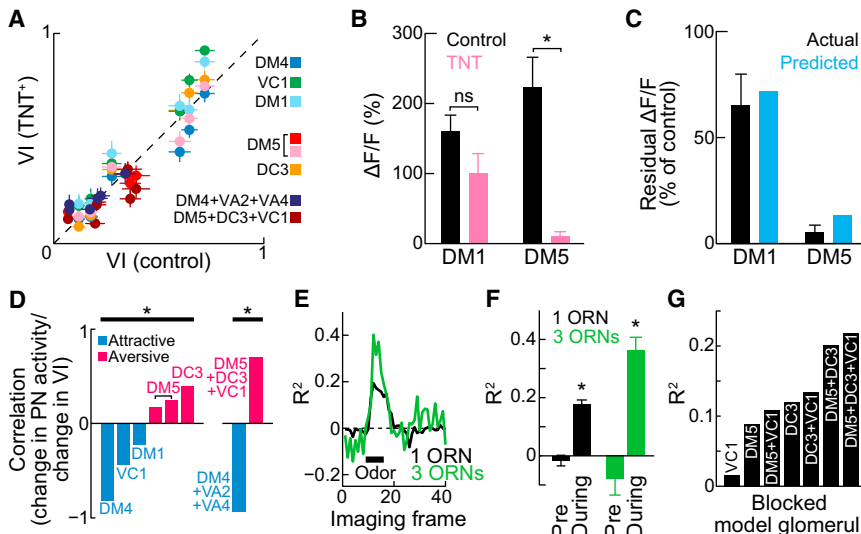


Figure 5. Behavioral Effect of Genetically Blocking Odor-Evoked Activity in Subsets of ORNs

(A) Comparison of VIs in TNT-positive (progeny of *Or-Gal4 × UAS-TNT*) and control (*UAS-TNT/+*) flies. Identity of glomeruli in which ORN output is blocked is indicated in color legend. Error bars show SEM across flies. Each genotype ($n = 21\text{--}26$ flies) was tested using a set of six odors, except DM5, which was tested with two odor sets (12 stimuli).

(B) Comparison of Ca^{2+} responses of the PNs in glomerulus DM1 and DM5 to ethyl acetate with or without TNT expression in their cognate ORNs (mean \pm SEM). TNT expression significantly reduced the response of DM5, but not DM1 PNs (two-sample t test, $p < 0.05$). DM5 response in TNT-expressing flies is not significantly different from zero (two-tailed t test, $p = 0.22$).

(C) Percentage of reduction in Ca^{2+} fluorescence due to TNT expression (data in B) compared with the predictions of a model in which ORN-PN synaptic transmission is blocked but PNs receive

excitatory input through lateral interactions between glomeruli. The prediction is computed from the Ca^{2+} responses recorded in GCaMP6f flies using an inferred PN-PN connection matrix (see Figure S5 and *Supplemental Experimental Procedures*).

(D) Pearson correlation between TNT-induced changes in PN activity and observed changes in behavioral response (six values for each condition; glomerulus DM5 tested with two different odor sets). Odor-evoked PN activity in TNT-positive flies is computed as in (C) and normalized according to the normalization model. The correlation of the pooled data was significant (two-tailed t test, $p < 0.01$), in both cases where either one (left) or three (right) ORN types were blocked.

(E) R^2 of predicted change in VI for the case where one or three ORN types were blocked, shown as a function of imaging time frame. Odor application period is indicated by a black bar (4 s).

(F) Mean prediction performance for the case where either one or three ORN types were blocked. The R^2 averaged over three consecutive imaging frames is shown before odor application (Pre, frames 3–5), and during odor application (During, frames 12–14). Error bars indicate SD over the three imaging frames. Asterisks indicate statistical significance ($p < 0.006$, permutation test).

(G) Prediction performance as a function of the identity of blocked glomeruli in the model, showing additive effects of glomerular blockade.

olfactory context. From the point of view of a PN, an olfactory context is characterized by a specific history, or profile, of activation, with different contexts giving rise to different activation profiles. In a hypothetical example shown in Figure 7A, an aversive glomerulus responds similarly to a set of odors in context A, thus making its activation profile narrow (top red histogram). The normalization procedure broadens this histogram (bottom red histogram), enhancing differences between odor responses (responses to odor 1 and 2 become more separated). On the other hand, the difference between odor responses becomes suppressed in an attractive glomerulus having an initial broad profile (top blue histogram). When considering valence integration over two glomeruli, odor 1 in this example is more attractive than odor 2 ($VI_2 - VI_1 > 0$). Intriguingly, if we assume mirror symmetric activation profiles in context B, odor 1 would become more aversive than odor 2, even though the glomerular responses to the two odors (indicated by large arrowheads) are identical in both contexts (only the contextual activation by other odors indicated by small arrowheads, differ). In sum, the relative valence of two odors may vary depending on the identity of the other odors presented in the same experiment. In the extreme, the preference between two odors may switch when sampled in particularly different contexts (Figure 7A).

To test whether this phenomenon actually occurs, we measured behavioral responses to five different odor pairs, each of which was tested in two different olfactory contexts consisting of four other odors (Figure 7B). We computed the relative

valence as the difference in VI between the two odors in the pair and tested whether and how the relative valence depended on the olfactory context. We found that the relative valence was indeed affected by the other odors in the set (Figure 7C). The observed changes were relatively small; however, the predictions of our model consistently matched the data, and this effect was statistically significant ($p < 0.03$, permutation test, Figure 7C). Remarkably, the relative valence switched sign in several cases, demonstrating that perceptual decisions can be modulated by the olfactory environment.

The accuracy of model predictions was robust. On average, the direction of change in relative valence was more accurately predicted as the number of glomeruli in the model increased (Figure 7D, left), indicating that this effect also depends on summing small contributions over many glomeruli. Moreover, the accuracy of the predictions correlated well with the prediction performance of the model (Figure 7D, right), showing that models that predict the valence of individual test odors well also tend to perform better at predicting contextual changes in relative valence.

To gain further insight into this phenomenon, we tested the influence of abruptly changing the olfactory context during the experiment. Using the same odor sets, we presented the first context during the first half of the experiment (trials 1–8) and switched to the second context during the second half (trials 9–15). This should in principle inform us on the timescale of adaptation to the olfactory context. When we compared these

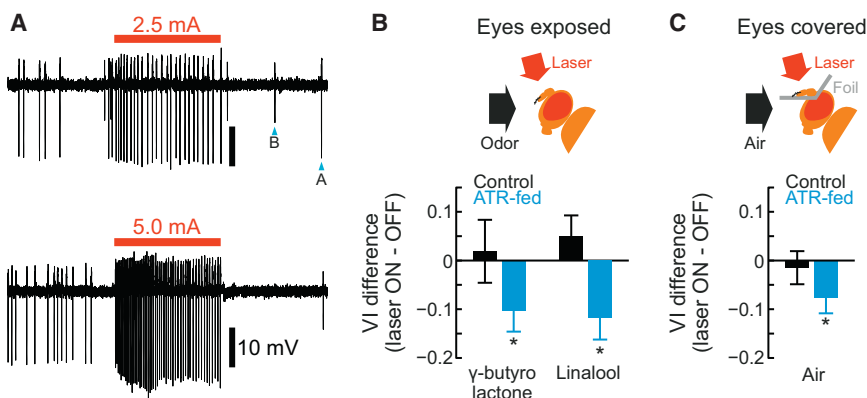


Figure 6. Optogenetic Activation of DM4 ORNs Evokes Attractive Behavior
(A) Responses of a Chrimson-expressing DM4 ORN (ab2A neuron) to a 637-nm laser light pulse at two different intensities. Red bar indicates period of laser application (1 s). Blue arrows denote the distinctive A and B spikes produced by the two neurons housed in the sensillum.
(B) Difference in VI between laser ON (5.0 mA) and laser OFF conditions in response to two odors, for Chrimson-positive ($n = 21$) and control ($n = 24$) flies (mean \pm SEM). Both are of the same genotype, *Or59b-Ga4;UAS-Chrimson*, but control flies were not fed all-trans retinal (ATR). ATR-fed flies show significantly more attractive responses when odors are paired with laser (Wilcoxon signed-rank test, Bonferroni-corrected, $p < 0.05$).
(C) Difference in VI between laser ON (12.5 mA) and laser OFF conditions without odorant stimulus, for ATR-positive ($n = 17$) and control ($n = 21$) flies (mean \pm SEM). Laser application was restricted to antennae by covering eyes and head cuticle with aluminum foil. ATR-positive flies show a significantly more attractive VI (Wilcoxon signed-rank test, $p < 0.05$).

data with the data obtained by sampling odor sets separately in different animals, we found that the results agreed: although changes in relative valence measured in the same animals tended to be smaller than those measured in different flies, the sign of the change was the same except for one case (Figure 7E). Interestingly, a model in which the relative valence of odors presented in the second half of the experiment is computed relative to a broader context, consisting of the sum of the first and second contexts, also predicts that the changes in relative valence should be smaller when the two contexts are presented sequentially (Figure S6). This suggests that in the second half of the experiment (10 to 20 min after the start of the experiment), flies are still affected by the odors sampled during the first 10 min, implying that adaptation occurs relatively slowly over a timescale of several minutes.

DISCUSSION

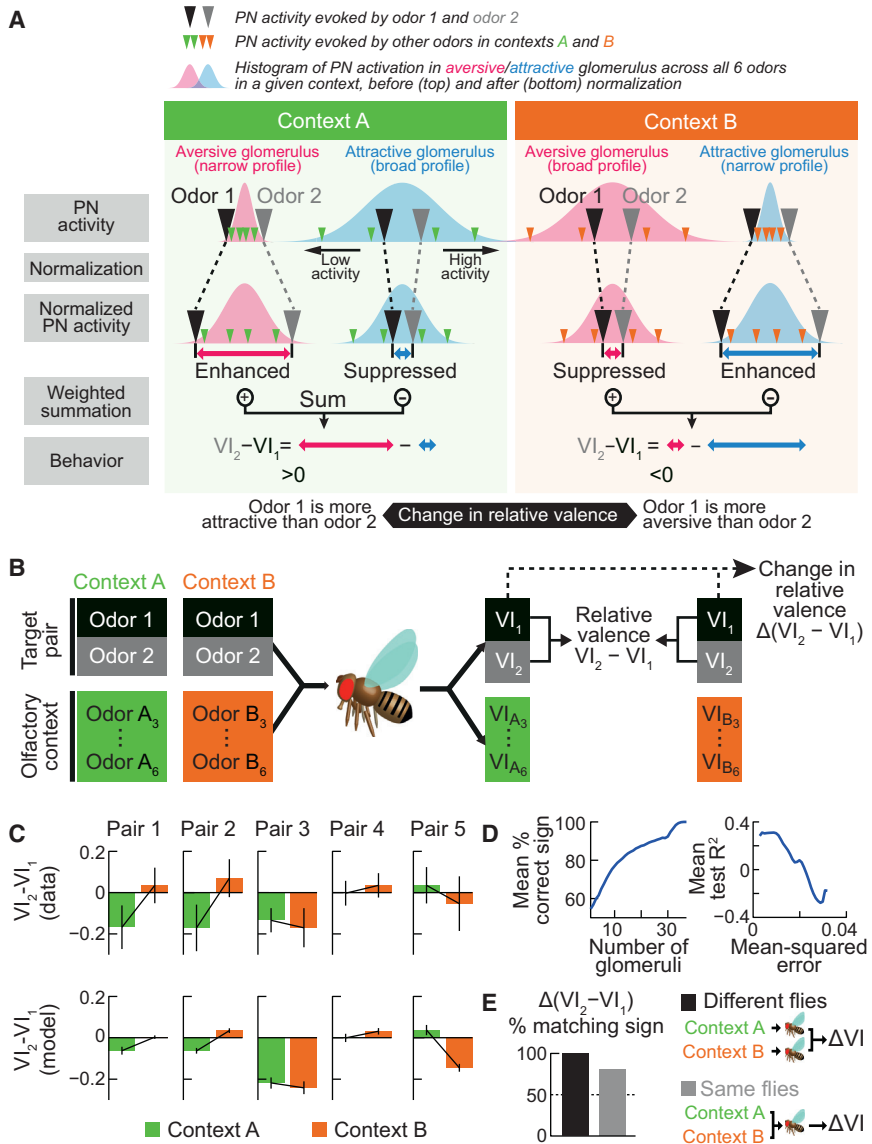
The aim of this study was to search for a general olfactory code—revealing the quantitative relationship between population neural activity and olfactory behavior that holds true for various odors under different contexts. Previous investigations have established how information about olfactory stimuli is encoded as patterns of glomerular activity in the olfactory bulb in vertebrates and the AL in insects. However, the computation that allows decoding of these activity patterns to guide behavior remained elusive. Here we present a model that can predict a fly's responses to novel odors and the way these responses adaptively change according to the olfactory environment.

A Decoding Model of Context-Dependent Olfactory Perception

There are several prerequisites for constructing a decoding model of perceptual performance. First, it is essential to obtain neuronal and behavioral data that are directly comparable. Most studies in *Drosophila* recorded transient neural activity in fixed preparations while scoring behavior integrated over an extended period of time in another setting (Knaden et al., 2012; Kreher et al., 2008; Parnas et al., 2013; Ronderos et al., 2014;

Semmelhack and Wang, 2009; Suh et al., 2004). Here, we made tethered individual flies navigate in a flight simulator so that identical, temporally aligned stimuli can be delivered during behavior and physiology experiments. A second requirement is to obtain physiological signals from a sufficiently large portion of neurons carrying the relevant sensory information. We took advantage of the *Drosophila* AL circuit, which is numerically and physically compact enough to be fully scanned by two-photon Ca^{2+} imaging, and whose outputs reach brain regions involved in memory and innate behaviors (Masse et al., 2009). Finally, it is necessary to cover a sufficiently large stimulus space, a requirement which is particularly stringent in olfaction where clearly defined axes for describing stimuli are lacking. We fulfilled these requirements by imaging PN dendritic activity in three quarters of the glomeruli at ~ 1.7 Hz, in response to 84 stimuli with diverse chemical structures, including binary mixtures and odorants at different concentrations. This comprehensive dataset (Table S2) could serve as a central counterpart of resources on odor representation by ORNs (Münch and Galizia, 2016).

Combining behavioral and physiological data allowed us to formulate a model explaining how behavioral responses can be decoded from glomerular activity. This simple model consists of a normalization step, operating independently on individual glomeruli, followed by a linear summation over all glomerular channels. Linear summation was naturally suggested by behavioral and physiological responses to binary mixtures and was sufficient to explain our data. Previous studies on mitral/tufted cells of the olfactory bulb and PNs of the insect AL reported results ranging from linear (Davison and Katz, 2007; Gupta et al., 2015; Khan et al., 2008) to non-linear interactions of the mixture components (Davison and Katz, 2007; Giraudet et al., 2002; Niessing and Friedrich, 2010; Shen et al., 2013; Tabor et al., 2004). However, because none of these studies examined behavior, it remained unknown whether glomerular output directly reflects innate olfactory perception. Here, we found that a linear model provided a good fit to the data. More importantly, behavioral responses mirrored the gradual change in PN activity. We do not claim, however, that non-linear interactions



the two contexts were sampled independently by different animals (same data as in C). Gray: “same flies” condition, in which the two contexts were presented sequentially to the same animals ($n = 40\text{--}41$ flies for each pair of odor sets). Dotted line indicates chance level (50%).

between glomeruli do not exist. For example, the efficacy of a glomerulus could be enhanced or depressed when it is co-activated with specific other channels. Nevertheless, given the accuracy of the linear framework, if such interactions do exist they are likely to be relatively weak or take effect in a stimulus range outside of our odor set.

A remarkable feature of our normalization model is its prediction that relative valence of odors can change depending on the olfactory environment. Behavioral experiments indeed showed that the fly’s relative odor preference scales, and even switches, in many cases. Normalization is ubiquitous in the brain (Carandini and Heeger, 2011), and also in the AL, where it is reportedly implemented by short-term depression at the ORN-PN synapse (Kazama and Wilson, 2008) and divisive inhibition within the AL

network (Olsen et al., 2010). We modeled normalization using mean subtraction and division by the SD, two widely used operations to explain neuronal adaptation occurring at a short timescale (Baccus and Meister, 2002; Chander and Chichilnisky, 2001; Nagel and Doupe, 2006; Ohzawa et al., 1985). Here, we show that this framework can also explain behavioral adaptation occurring over a longer timescale.

It would be of interest to determine where and how the normalization operation described here takes place in the olfactory circuit. Mean subtraction is a form of high-pass filtering, which could be implemented through short-term synaptic plasticity (Abbott and Regehr, 2004), for example at synapses between PNs and third-order neurons. Alternatively, it may be supported by spike-frequency adaptation (Benda and Herz, 2003). For the

Figure 7. The Relative Valence of Pairs of Odors Depends on the Olfactory Context

(A) Description of a hypothetical mechanism underlying context-dependent changes in relative valence in the normalization model. Different olfactory contexts are characterized by different profiles of PN activation, represented as Gaussians, determined by PN responses to the six odors in the context (arrowheads). According to the model, the attractive or aversive effect of a PN is enhanced if its activation profile in a given context is narrow, but weakened if it is broad (see text for details). As a consequence, the relative VI ($VI_2 - VI_1$), determined by summing differences in normalized PN activity over glomeruli, becomes context dependent.

(B) Schematic of experimental procedure. Two odor sets are prepared that include a pair of odors in common (odor 1 and 2). The remaining four odors define the olfactory context. Behavioral responses to both sets are measured independently, and the relative valence of the common odors is computed for each set as the difference in VIs ($VI_2 - VI_1$). The context-dependent change in relative valence is defined as the difference in this value between two contexts $\Delta(VI_2 - VI_1)$.

(C) Comparison of observed changes in relative valence with predictions of the normalization model, showing good agreement ($p < 0.03$, permutation test). Five odor pairs were obtained using four odor sets ($n = 21\text{--}23$ flies for each set). Pair 1: methanoic acid/1-octanol. Pair 2: methanoic acid/acetophenone. Pair 3: 1-octanol/acetophenone. Pair 4: 2-butanone/1-butanol. Pair 5: methanoic acid/1-butanol. Error bars show SEM (top, across tested flies; bottom, across 9 sets of glomerulus weights obtained in cross-validation). (D) Left: average percentage of correctly predicted signs of change in relative valence, as a function of the number of glomeruli included in the model. Right: average prediction performance of the model as a function of the mean-square error on the prediction of changes in relative valence.

(E) Percentage of odor pairs for which the direction of change in relative valence was correctly predicted. Black: “different flies” condition, in which the two contexts were presented sequentially to different animals. Gray: “same flies” condition, in which the two contexts were presented sequentially to the same animals.

divisive component, it is not immediately obvious how a standard deviation could be computed; however, alternative models are possible. For example, in our data the SD correlated highly with the maximal activity, so that a model that rescales glomerular efficacy by the maximal activation performs equally well (data not shown). This simple form of gain control might be implementable, for example, by slow synaptic depression (Rothman et al., 2009). Although our data do not allow us to specify the exact mechanism of normalization, a nonlinear processing step is necessary to explain context-dependent changes in relative valence.

Rapid Odor Valuation by Tethered Flies

Earlier studies using tethered flies characterized how they modulate their flight upon encountering olfactory cues, but with few odors (Bhandawat et al., 2010; Frye and Dickinson, 2004; Guo and Guo, 2005; Wolf and Heisenberg, 1991). It therefore remained unexplored whether flies express fixed or graded responses depending on olfactory identity. We exposed flies to a large panel of odors and found a spectrum of responses. This suggests that flies are able to discriminate various odors and take graded actions. The difference in initial response was manifest within several hundreds of ms, demonstrating that flies can not only detect but also interpret odors rapidly. This initial decision correlated with the proportion of time spent outside the odor after prolonged exploration, suggesting that it reflects innate odor valuation. The short timescale of perceptual decision parallels that of the rodent's single sniff, which is sufficient to discriminate odors (Uchida and Mainen, 2003; Wesson et al., 2008). Given that odors in a natural environment are found in the form of plumes, which a navigating fly can cross in an instant (Murlis et al., 1992), the duration of each odor sampling may be comparable to, or even shorter than, a sniff. Therefore, rapid odor valuation is likely to be a fundamental requirement for efficient odor-guided navigation in complex environments.

Coding of Odor Valence by Individual Glomeruli

Previous research identified a number of glomeruli that appear dedicated to processing specific odorants such as pheromones, or broader classes of odors such as acids (reviewed in Li and Libeles, 2015). In all cases, silencing the glomerulus inhibited a behavioral response, suggesting that information about the valence of the tested stimuli is exclusively encoded in the activity of these glomeruli. However, because these studies generally used few odorants, and only a small fraction of glomeruli were tested, it is unclear how these results generalize to broader odor sets, and whether similar conclusions may hold for each of the ~50 glomeruli.

Our model attributes a specific weight to each glomerulus; the valence of a glomerulus thus corresponds to the sign of the associated weight. This model accurately fitted the data and predicted responses to novel odors. However, this does not entail that a causal relationship exists between glomerular activity and behavioral responses. We therefore tested causality by genetically blocking ORN input to targeted glomeruli, and by optically enhancing ORN input to a single glomerulus. The resulting changes in behavior were broadly consistent with the predictions of our model. Furthermore, when we compared glomerular valences obtained in our analysis with published data in which a causal link was demonstrated, we found that both agreed in most cases. Attraction was previously linked to the activation of DM1 and VA2 (Semmelhack and Wang, 2009), VM1 (Min et al., 2013), DC3 (Ronderos et al., 2014), and DA1 and VA6 (Schlief and Wilson, 2007). Conversely, DA2 (Stensmyr et al., 2012), DM5 (Semmelhack and Wang, 2009), and DM2 (Gao et al., 2015) were reported to mediate aversive responses. Our data differ from these results in only two cases, DC3 and VA6, both of which are of aversive valence in our model. It should be noted, however, that although DC3 was shown to subserve attraction to farnesol in Ronderos et al. (2014), another study (Knaden et al., 2012) reported DC3 to be activated almost exclusively by aversive odorants. Moreover, the study reporting VA6-mediated attraction to geranyl acetate (Schlief and Wilson, 2007) also found that it mediated aversive responses to higher concentrations of the same odorant. Our results are thus in agreement with the published literature, supporting the validity of our model.

Integration of Valence Information over Multiple Glomerular Channels

Although a causal effect on behavior had been demonstrated for some glomeruli, it remained unclear whether animals make decisions based on the entire AL output, or rely on a smaller subset of specialized glomeruli. Four lines of evidence in our data support the hypothesis that behavioral responses result from integrating valence information over a large number of glomerular channels. First, the predictive power of the model increased as more glomeruli were added to the set of independent variables. Second, genetically blocking synaptic input to subsets of glomeruli had small and graded effects on behavior. This observation is in line with a previous study of odor discrimination (Parnas et al., 2013), in which silencing subsets of glomeruli evoked graded behavioral effects. Third, blocking input to every tested glomerulus biased behavior in a direction consistent with the model. Fourth, the extent of this behavioral bias was quantitatively predicted by our population decoding model.

Our model naturally accounts for findings on the processing of both specific and general odors: whereas behavioral responses to odors that exclusively activate narrowly tuned receptors can be explained solely by the activity of the corresponding glomeruli, responses to general odors recruiting multiple receptors need to be explained by an integrated output from the activated glomerular ensemble.

In *Drosophila*, innate olfactory behavior depends primarily on the lateral horn (LH), one of two brain regions postsynaptic to the AL (de Belle and Heisenberg, 1994; Heimbeck et al., 2001; Parnas et al., 2013). The LH is innervated by the excitatory PNs examined in the present study and by inhibitory PNs (iPNs; Liang et al., 2013; Parnas et al., 2013; Strutz et al., 2014; Wang et al., 2014). Whereas one study reported that a subset of iPNs responds differentially to attractive and aversive odors and contributes to behavioral expression (Strutz et al., 2014), another study (Parnas et al., 2013) found no effect of iPNs on innate responses, suggesting a major role of excitatory PNs in odor valuation. A better view on the interaction between these pathways

requires studying how the population code described here in the AL is transformed in the LH.

EXPERIMENTAL PROCEDURES

Fly Stocks

Flies were raised on conventional cornmeal agar medium under a 12 hr light/12 hr dark cycle at 25°C. Experiments were performed on 2- to 4-day-old adult females. Flies were starved for 4–6 hr with water prior to experiments. Flies used in the study are listed in [Table S3](#).

Olfactory Stimulation

Odors were delivered by passing an air stream through 4 mL of odorant solution in a vial. A portion of the air stream was delivered through a 0.2 mm outlet placed 10 mm from the fly. Air flow was set to 0.3 m/s at fly location. A total of 84 odors were used ([Table S1](#)).

Behavioral Experiments

Flies were cold anesthetized, tethered to a stainless steel pin, and transferred to the flight simulator, which consisted of an odor delivery apparatus and a semi-circular array of green LEDs. The setup was enclosed in an opaque container and the fly was visualized using an infrared camera.

Flight behavior was monitored using two microphones positioned laterally ~1 mm from the tip of the extended wing on either side of the fly, whose outputs were analyzed in real time to extract turning direction and speed. The validity of computing turning propensity from microphone data was verified by comparing with video data ([Figure S1](#)). The visual stimulus (essential to increase flight reliability) consisted of vertical gratings with 60 deg⁻¹ spatial frequency. The panel of 84 odors was divided in sets of 6 ([Table S1](#)) and a single set was applied in each experiment (except [Figure 7E](#), “same flies” condition, where two sets were applied consecutively). The protocol consisted of 15 blocks, in which each of the 6 odors plus mineral oil were applied in randomized order, up to a fixed duration (4 s unless otherwise stated) and in a restricted spatial region (45° centered at the fly location at the time of odor contact). Odor application was terminated when the fly exited this region and re-initiated upon re-entry within the application period. For optogenetic activation experiments, a 637 nm laser targeted at the antennae was controlled in closed-loop similarly as odorant stimuli.

Two-Photon Imaging

Individual flies were attached to a custom recording plate with ultraviolet-curing adhesive while cold-anesthetized. Saline bubbled with 95% O₂/5% CO₂ was added and the head cuticle was removed to expose the brain.

The entire right AL was imaged with a two-photon laser scanning microscope. The fluorophore was excited with a titanium:sapphire pulsed laser mode locked at 930 nm. Each odor was presented for 4 s with 1 min inter-trial interval. Odor valve opened in frame 9 and closed in frame 16. Each odor was presented four times in randomized order as in behavioral experiments. After data collection, a high-resolution 3D image of the AL comprising 99 optical slices (1 μm interval) was acquired for offline identification of guide-post glomeruli (see [Data Analysis](#) section).

Data Analysis

Behavioral Data Analysis

Valence indices (VIs) for individual flies were obtained by aligning flight trajectories to the time of odor contact ([Figure S7](#)) and calculating the proportion of time spent outside the plume. Instantaneous VIs were calculated in every 5 ms time bin, and the mean VI (simply referred to as VI throughout the text) was calculated as an average over the last 1 s of odor presentation. Mean and standard error were computed by pooling all tested flies. ΔWBA in [Figure 1G](#) was calculated using the absolute difference in the standardized wing-beat amplitudes ([Supplemental Experimental Procedures](#)). Trials in which flight was interrupted were excluded.

Two-Photon Imaging Data Analysis

Images were analyzed in three steps: correction for brain motion, creation of template glomeruli, and extraction of fluorescence changes in each glomer-

ulus using the template ([Figure S3](#)). [Table S2](#) summarizes the mean response of each of the 37 glomeruli to the 84 odors in our dataset.

Decoding Analysis

For the normalization model, PN data were standardized in each glomerulus using mean and standard deviation values computed independently for each set of six odors, by pooling trial-averaged ΔF/F responses (imaging frames 12 to 16) over all six odors. VI values were similarly centered by subtracting their mean value over the six odors. The model was fit using partial least-squares regression and a cross-validation procedure to control for overfitting. Prediction performance was assessed using the R² coefficient and statistical significance using a permutation test.

See [Supplemental Experimental Procedures](#) for detailed methods.

SUPPLEMENTAL INFORMATION

Supplemental Information includes Supplemental Experimental Procedures, seven figures, three tables, and two movies and can be found with this article online at <http://dx.doi.org/10.1016/j.neuron.2016.05.022>.

AUTHOR CONTRIBUTIONS

L.B. and H.K. conceived and designed the study. L.B. and H.K. constructed the flight simulator with input from Hiroshi M. Shiozaki, and the olfactometer with input from Keita Endo. L.B. and K.O. performed behavioral experiments and analyzed data. Y.T. and H.K. performed imaging experiments and analyzed data. L.B. performed single sensillum recordings. L.B. and H.K. performed decoding analyses and wrote the manuscript.

ACKNOWLEDGMENTS

We thank Vivek Jayaraman, Christopher Potter, Hiromu Tanimoto, Rachel Wilson, the Bloomington Stock Center, and the Developmental Studies Hybridoma Bank for fly stocks and reagents; Justin Gardner, Matthieu Louis, Taro Toyoizumi, and Naoshige Uchida for comments on the manuscript; members of the H.K. laboratory for their support and comments on the manuscript. This work was supported by a grant from RIKEN and Grants-in-Aid for Scientific Research (23680044, 25115732) from MEXT (to H.K.). L.B. was partially supported by grant PA00P3_139660 from the Swiss National Science Foundation.

Received: August 21, 2015

Revised: March 22, 2016

Accepted: May 11, 2016

Published: June 16, 2016

REFERENCES

- Abbott, L.F., and Regehr, W.G. (2004). Synaptic computation. *Nature* **431**, 796–803.
- Ai, M., Min, S., Grosjean, Y., Leblanc, C., Bell, R., Benton, R., and Suh, G.S.B. (2010). Acid sensing by the *Drosophila* olfactory system. *Nature* **468**, 691–695.
- Baccus, S.A., and Meister, M. (2002). Fast and slow contrast adaptation in retinal circuitry. *Neuron* **36**, 909–919.
- Benda, J., and Herz, A.V. (2003). A universal model for spike-frequency adaptation. *Neural Comput.* **15**, 2523–2564.
- Bhandawat, V., Maimon, G., Dickinson, M.H., and Wilson, R.I. (2010). Olfactory modulation of flight in *Drosophila* is sensitive, selective and rapid. *J. Exp. Biol.* **213**, 3625–3635.
- Carandini, M., and Heeger, D.J. (2011). Normalization as a canonical neural computation. *Nat. Rev. Neurosci.* **13**, 51–62.
- Chander, D., and Chichilnisky, E.J. (2001). Adaptation to temporal contrast in primate and salamander retina. *J. Neurosci.* **21**, 9904–9916.
- Chen, T.-W., Wardill, T.J., Sun, Y., Pulver, S.R., Renninger, S.L., Baohan, A., Schreiter, E.R., Kerr, R.A., Orger, M.B., Jayaraman, V., et al. (2013). Ultrasensitive fluorescent proteins for imaging neuronal activity. *Nature* **499**, 295–300.

- Clepce, M., Neumann, K., Martus, P., Nitsch, M., Wielopolski, J., Koch, A., Kornhuber, J., Reich, K., and Thuerauf, N. (2014). The psychophysical assessment of odor valence: does an anchor stimulus influence the hedonic evaluation of odors? *Chem. Senses* 39, 17–25.
- Couto, A., Alenius, M., and Dickson, B.J. (2005). Molecular, anatomical, and functional organization of the *Drosophila* olfactory system. *Curr. Biol.* 15, 1535–1547.
- Cury, K.M., and Uchida, N. (2010). Robust odor coding via inhalation-coupled transient activity in the mammalian olfactory bulb. *Neuron* 68, 570–585.
- Davison, I.G., and Katz, L.C. (2007). Sparse and selective odor coding by mitral/tufted neurons in the main olfactory bulb. *J. Neurosci.* 27, 2091–2101.
- de Belle, J.S., and Heisenberg, M. (1994). Associative odor learning in *Drosophila* abolished by chemical ablation of mushroom bodies. *Science* 263, 692–695.
- Dweck, H.K., Ebrahim, S.A., Kromann, S., Bown, D., Hillbur, Y., Sachse, S., Hansson, B.S., and Stensmyr, M.C. (2013). Olfactory preference for egg laying on citrus substrates in *Drosophila*. *Curr. Biol.* 23, 2472–2480.
- Fishilevich, E., and Vosshall, L.B. (2005). Genetic and functional subdivision of the *Drosophila* antennal lobe. *Curr. Biol.* 15, 1548–1553.
- Friedrich, R.W., and Korschning, S.I. (1997). Combinatorial and chemotopic odorant coding in the zebrafish olfactory bulb visualized by optical imaging. *Neuron* 18, 737–752.
- Friedrich, R.W., and Laurent, G. (2001). Dynamic optimization of odor representations by slow temporal patterning of mitral cell activity. *Science* 291, 889–894.
- Frye, M.A., and Dickinson, M.H. (2004). Motor output reflects the linear superposition of visual and olfactory inputs in *Drosophila*. *J. Exp. Biol.* 207, 123–131.
- Gao, X.J., Clandinin, T.R., and Luo, L. (2015). Extremely sparse olfactory inputs are sufficient to mediate innate aversion in *Drosophila*. *PLoS ONE* 10, e0125986.
- Giraudet, P., Berthommier, F., and Chaput, M. (2002). Mitral cell temporal response patterns evoked by odor mixtures in the rat olfactory bulb. *J. Neurophysiol.* 88, 829–838.
- Guo, J., and Guo, A. (2005). Crossmodal interactions between olfactory and visual learning in *Drosophila*. *Science* 309, 307–310.
- Gupta, P., Albeau, D.F., and Bhalla, U.S. (2015). Olfactory bulb coding of odors, mixtures and sniffs is a linear sum of odor time profiles. *Nat. Neurosci.* 18, 272–281.
- Hallez, E.A., and Carlson, J.R. (2006). Coding of odors by a receptor repertoire. *Cell* 125, 143–160.
- Heimbeck, G., Bugnon, V., Gendre, N., Keller, A., and Stocker, R.F. (2001). A central neural circuit for experience-independent olfactory and courtship behavior in *Drosophila melanogaster*. *Proc. Natl. Acad. Sci. USA* 98, 15336–15341.
- Joerges, J., Kuttner, A., Galizia, C.G., and Menzel, R. (1997). Representations of odours and odour mixtures visualized in the honeybee brain. *Nature* 387, 285–288.
- Kazama, H., and Wilson, R.I. (2008). Homeostatic matching and nonlinear amplification at identified central synapses. *Neuron* 58, 401–413.
- Kazama, H., and Wilson, R.I. (2009). Origins of correlated activity in an olfactory circuit. *Nat. Neurosci.* 12, 1136–1144.
- Khan, A.G., Thattai, M., and Bhalla, U.S. (2008). Odor representations in the rat olfactory bulb change smoothly with morphing stimuli. *Neuron* 57, 571–585.
- Klapoetke, N.C., Murata, Y., Kim, S.S., Pulver, S.R., Birdsey-Benson, A., Cho, Y.K., Morimoto, T.K., Chuong, A.S., Carpenter, E.J., Tian, Z., et al. (2014). Independent optical excitation of distinct neural populations. *Nat. Methods* 11, 338–346.
- Knaden, M., Strutz, A., Ahsan, J., Sachse, S., and Hansson, B.S. (2012). Spatial representation of odorant valence in an insect brain. *Cell Rep.* 1, 392–399.
- Kohn, A. (2007). Visual adaptation: physiology, mechanisms, and functional benefits. *J. Neurophysiol.* 97, 3155–3164.
- Kreher, S.A., Mathew, D., Kim, J., and Carlson, J.R. (2008). Translation of sensory input into behavioral output via an olfactory system. *Neuron* 59, 110–124.
- Li, Q., and Liberles, S.D. (2015). Aversion and attraction through olfaction. *Curr. Biol.* 25, R120–R129.
- Liang, L., Li, Y., Potter, C.J., Yizhar, O., Deisseroth, K., Tsien, R.W., and Luo, L. (2013). GABAergic projection neurons route selective olfactory inputs to specific higher-order neurons. *Neuron* 79, 917–931.
- Lin, C.C., Prokop-Prigge, K.A., Preti, G., and Potter, C.J. (2015). Food odors trigger *Drosophila* males to deposit a pheromone that guides aggregation and female oviposition decisions. *eLife* 4, e08688.
- Louie, K., Khaw, M.W., and Glimcher, P.W. (2013). Normalization is a general neural mechanism for context-dependent decision making. *Proc. Natl. Acad. Sci. USA* 110, 6139–6144.
- Malnic, B., Hirono, J., Sato, T., and Buck, L.B. (1999). Combinatorial receptor codes for odors. *Cell* 96, 713–723.
- Masse, N.Y., Turner, G.C., and Jefferis, G.S.X.E. (2009). Olfactory information processing in *Drosophila*. *Curr. Biol.* 19, R700–R713.
- Min, S., Ai, M., Shin, S.A., and Suh, G.S.B. (2013). Dedicated olfactory neurons mediating attraction behavior to ammonia and amines in *Drosophila*. *Proc. Natl. Acad. Sci. USA* 110, E1321–E1329.
- Münch, D., and Galizia, C.G. (2016). Door 2.0 - comprehensive mapping of *Drosophila melanogaster* odorant responses. *Sci. Rep.* 6, 21841.
- Murlis, J., Elkinton, J.S., and Carde, R.T. (1992). Odor plumes and how insects use them. *Annu. Rev. Entomol.* 37, 505–532.
- Nagel, K.I., and Doupe, A.J. (2006). Temporal processing and adaptation in the songbird auditory forebrain. *Neuron* 51, 845–859.
- Ng, M., Roorda, R.D., Lima, S.Q., Zemelman, B.V., Morcillo, P., and Miesenböck, G. (2002). Transmission of olfactory information between three populations of neurons in the antennal lobe of the fly. *Neuron* 36, 463–474.
- Niessing, J., and Friedrich, R.W. (2010). Olfactory pattern classification by discrete neuronal network states. *Nature* 465, 47–52.
- Ohzawa, I., Sclar, G., and Freeman, R.D. (1985). Contrast gain control in the cat's visual system. *J. Neurophysiol.* 54, 651–667.
- Olsen, S.R., Bhandawat, V., and Wilson, R.I. (2007). Excitatory interactions between olfactory processing channels in the *Drosophila* antennal lobe. *Neuron* 54, 89–103.
- Olsen, S.R., Bhandawat, V., and Wilson, R.I. (2010). Divisive normalization in olfactory population codes. *Neuron* 66, 287–299.
- Parnas, M., Lin, A.C., Huettroth, W., and Miesenböck, G. (2013). Odor discrimination in *Drosophila*: from neural population codes to behavior. *Neuron* 79, 932–944.
- Potter, C.J., Tasic, B., Russler, E.V., Liang, L., and Luo, L. (2010). The Q system: a repressible binary system for transgene expression, lineage tracing, and mosaic analysis. *Cell* 141, 536–548.
- Ronderos, D.S., Lin, C.C., Potter, C.J., and Smith, D.P. (2014). Farnesol-detecting olfactory neurons in *Drosophila*. *J. Neurosci.* 34, 3959–3968.
- Root, C.M., Semmelhack, J.L., Wong, A.M., Flores, J., and Wang, J.W. (2007). Propagation of olfactory information in *Drosophila*. *Proc. Natl. Acad. Sci. USA* 104, 11826–11831.
- Rothman, J.S., Cathala, L., Steuber, V., and Silver, R.A. (2009). Synaptic depression enables neuronal gain control. *Nature* 457, 1015–1018.
- Rubin, B.D., and Katz, L.C. (1999). Optical imaging of odorant representations in the mammalian olfactory bulb. *Neuron* 23, 499–511.
- Schlief, M.L., and Wilson, R.I. (2007). Olfactory processing and behavior downstream from highly selective receptor neurons. *Nat. Neurosci.* 10, 623–630.
- Semmelhack, J.L., and Wang, J.W. (2009). Select *Drosophila* glomeruli mediate innate olfactory attraction and aversion. *Nature* 459, 218–223.
- Shang, Y., Claridge-Chang, A., Sjulson, L., Pypaert, M., and Miesenböck, G. (2007). Excitatory local circuits and their implications for olfactory processing in the fly antennal lobe. *Cell* 128, 601–612.

- Shen, K., Tootoonian, S., and Laurent, G. (2013). Encoding of mixtures in a simple olfactory system. *Neuron* 80, 1246–1262.
- Spors, H., and Grinvald, A. (2002). Spatio-temporal dynamics of odor representations in the mammalian olfactory bulb. *Neuron* 34, 301–315.
- Stensmyr, M.C., Dweck, H.K.M., Farhan, A., Ibba, I., Strutz, A., Mukunda, L., Linz, J., Grabe, V., Steck, K., Lavista-Llanos, S., et al. (2012). A conserved dedicated olfactory circuit for detecting harmful microbes in *Drosophila*. *Cell* 151, 1345–1357.
- Strutz, A., Soelter, J., Baschwitz, A., Farhan, A., Grabe, V., Rybak, J., Knaden, M., Schmuker, M., Hansson, B.S., and Sachse, S. (2014). Decoding odor quality and intensity in the *Drosophila* brain. *eLife* 3, e04147.
- Suh, G.S., Wong, A.M., Hergarden, A.C., Wang, J.W., Simon, A.F., Benzer, S., Axel, R., and Anderson, D.J. (2004). A single population of olfactory sensory neurons mediates an innate avoidance behaviour in *Drosophila*. *Nature* 431, 854–859.
- Sweeney, S.T., Broadie, K., Keane, J., Niemann, H., and O’Kane, C.J. (1995). Targeted expression of tetanus toxin light chain in *Drosophila* specifically eliminates synaptic transmission and causes behavioral defects. *Neuron* 14, 341–351.
- Tabor, R., Yaksi, E., Weislogel, J.M., and Friedrich, R.W. (2004). Processing of odor mixtures in the zebrafish olfactory bulb. *J. Neurosci.* 24, 6611–6620.
- Tanaka, N.K., Endo, K., and Ito, K. (2012). Organization of antennal lobe-associated neurons in adult *Drosophila melanogaster* brain. *J. Comp. Neurol.* 520, 4067–4130.
- Thum, A.S., Jenett, A., Ito, K., Heisenberg, M., and Tanimoto, H. (2007). Multiple memory traces for olfactory reward learning in *Drosophila*. *J. Neurosci.* 27, 11132–11138.
- Tian, L., Hires, S.A., Mao, T., Huber, D., Chiappe, M.E., Chalasani, S.H., Petreanu, L., Akerboom, J., McKinney, S.A., Schreiter, E.R., et al. (2009). Imaging neural activity in worms, flies and mice with improved GCaMP calcium indicators. *Nat. Methods* 6, 875–881.
- Tully, T., and Quinn, W.G. (1985). Classical conditioning and retention in normal and mutant *Drosophila melanogaster*. *J. Comp. Physiol. A Neuroethol. Sens. Neural Behav. Physiol.* 157, 263–277.
- Uchida, N., and Mainen, Z.F. (2003). Speed and accuracy of olfactory discrimination in the rat. *Nat. Neurosci.* 6, 1224–1229.
- Uchida, N., Takahashi, Y.K., Tanifuji, M., and Mori, K. (2000). Odor maps in the mammalian olfactory bulb: domain organization and odorant structural features. *Nat. Neurosci.* 3, 1035–1043.
- Vosshall, L.B., Wong, A.M., and Axel, R. (2000). An olfactory sensory map in the fly brain. *Cell* 102, 147–159.
- Wang, J.W., Wong, A.M., Flores, J., Vosshall, L.B., and Axel, R. (2003). Two-photon calcium imaging reveals an odor-evoked map of activity in the fly brain. *Cell* 112, 271–282.
- Wang, K., Gong, J., Wang, Q., Li, H., Cheng, Q., Liu, Y., Zeng, S., and Wang, Z. (2014). Parallel pathways convey olfactory information with opposite polarities in *Drosophila*. *Proc. Natl. Acad. Sci. USA* 111, 3164–3169.
- Wark, B., Lundstrom, B.N., and Fairhall, A. (2007). Sensory adaptation. *Curr. Opin. Neurobiol.* 17, 423–429.
- Wehr, M., and Laurent, G. (1996). Odour encoding by temporal sequences of firing in oscillating neural assemblies. *Nature* 384, 162–166.
- Wesson, D.W., Carey, R.M., Verhagen, J.V., and Wachowiak, M. (2008). Rapid encoding and perception of novel odors in the rat. *PLoS Biol.* 6, e82.
- Wolf, R., and Heisenberg, M. (1991). Basic organization of operant behavior as revealed in *Drosophila* flight orientation. *J. Comp. Physiol. A Neuroethol. Sens. Neural Behav. Physiol.* 169, 699–705.

Neuron, Volume 91

Supplemental Information

Decoding of Context-Dependent Olfactory

Behavior in *Drosophila*

Laurent Badel, Kazumi Ohta, Yoshiko Tsuchimoto, and Hokto Kazama

CONTENTS

Figure S1 (related to Figure 1)	<i>Measurement and characterization of odor-evoked behavioral responses</i>
Figure S2 (related to Figure 1)	<i>Behavioral effect of genetically blocking synaptic transmission in Orco-dependent ORNs</i>
Figure S3 (related to Figure 2)	<i>Characterization of the accuracy of the image registration procedure</i>
Figure S4 (related to Figure 2)	<i>Linear correlations between PN and behavioral responses</i>
Figure S5 (related to Figure 5)	<i>PN-PN connectivity inferred from Ca^{2+} imaging data</i>
Figure S6 (related to Figure 7)	<i>Comparison of model predictions for the change in relative valence as a function of the breadth of the olfactory context</i>
Figure S7 (related to Experimental Procedures)	<i>Characterization of the odor delivery system</i>
Table S1 (related to Figure 1)	<i>List of odors used in the study</i>
Table S2 (related to Figure 2)	<i>Mean Ca^{2+} responses of PNs in 37 glomeruli to a set of 84 odors (legend)</i>
Table S3 (related to Experimental Procedures)	<i>List of genotypes used in the study and associated RRIDs</i>
Movie S1 (related to Figure 1)	<i>Reconstruction of a behavioral trial exemplifying aversive and attractive responses. (legend)</i>
Movie S2 (related to Figure 2)	<i>Representative odor response of PNs (legend).</i>
Supplemental Experimental Procedures	
Supplemental References	

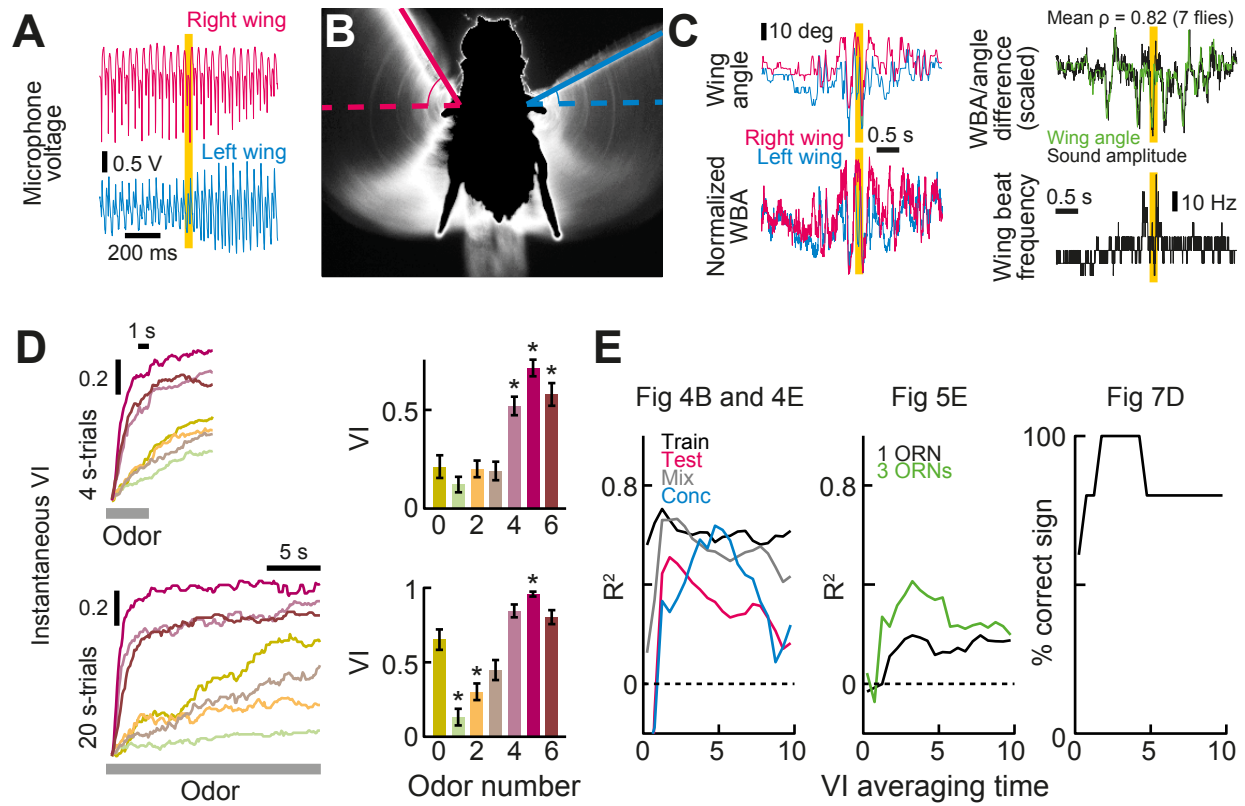


Figure S1 (related to Figure 1). Measurement and characterization of odor-evoked behavioral responses

(A) Sample raw sound data recorded with the left and right microphones. Each wing beat evokes a sharp peak in the microphone voltage with varying amplitude.

(B) Sample snapshot taken using the IR camera and illustration of the left and right wing angles.

(C) Left: wing angles extracted from video (top) and wing-beat amplitudes extracted from sound (bottom) data. Top right: the difference in wing beat amplitudes, which was used to update the heading direction, is highly correlated with the difference in wing angles (average correlation coefficient calculated over 6 s of data in 7 flies, $\rho = 0.82$). Bottom right: the wing-beat frequency is also accessible from sound data. The vertical yellow lines in A and C correspond to the time of the snapshot in B.

(D) Comparison of behavioral responses to 4 s- and 20 s-long odor presentations. Left: instantaneous valence index (VI, proportion of time spent outside of the odor plume) as a function of the time since odor onset. All odors evoke monotonic increases that are faster for aversive (4-6 in right graph) than attractive (1-3) odors. Attractive odors differentiate better from the control odor (0, mineral oil) after extended sampling. Right: the VI is obtained by averaging this quantity in a specified time window (top: 3-4 s, bottom: 15-20 s after odor onset). Error bars denote SEM across flies ($n = 21-22$). Asterisks indicate statistically different values from the mineral oil control (odor 0; Mann-Whitney U-test, Bonferroni corrected, $p < 0.05$). Odor color code is the same as in Figure 1.

(E) Model performance as a function of the time interval used to average VI values. Here, mean VIs are calculated by averaging the instantaneous VI in 0.5 s-time windows, and these values are used to repeat the analyses of Figures 4B and 4E (left), 5E (middle) and 7D (right).

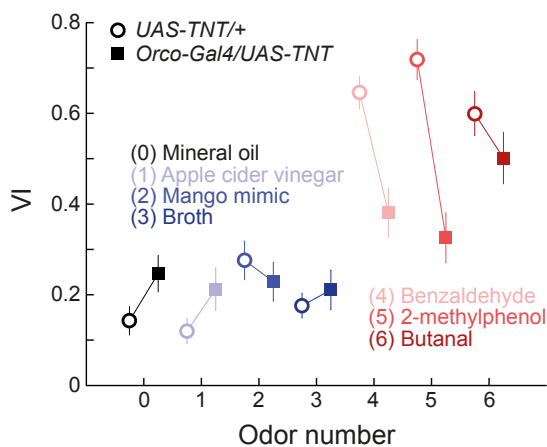
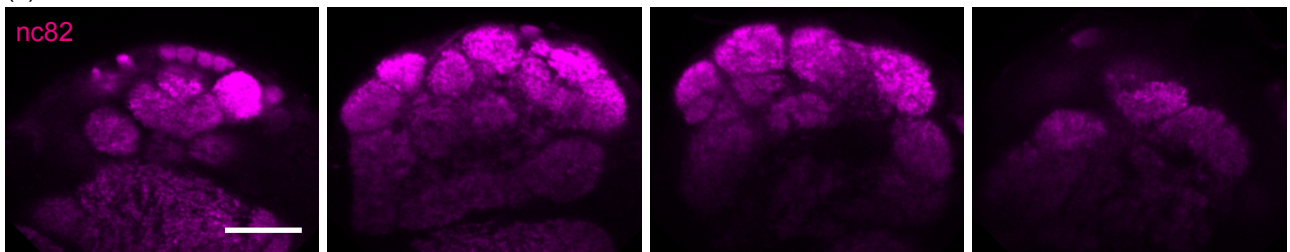


Figure S2 (related to Figure 1). Behavioral effect of genetically blocking synaptic transmission in Orco-dependent ORNs

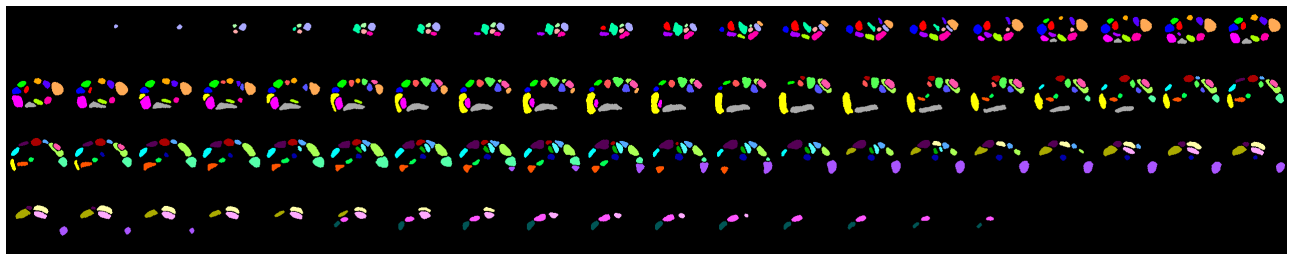
Behavioral responses to mineral oil (black), 3 attractive (blue) and 3 aversive (red) odors are compared across 2 genetic strains: a control strain (*UAS-TNT*+/+, open circles) and a strain expressing tetanus toxin (TNT), a blocker of synaptic transmission, in the majority of ORNs (*Orco-Gal4/UAS-TNT*, filled squares). Error bars represent SEM (n = 22 flies for each genotype).

A

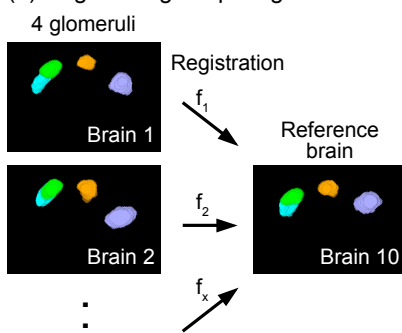
(1) Stain individual brains with antibodies



(2) Delineate the 37 NP225-Ga4-positive glomeruli



(3) Register 4 guidepost glomeruli



(4) Apply the same transformation to all glomeruli and create the template

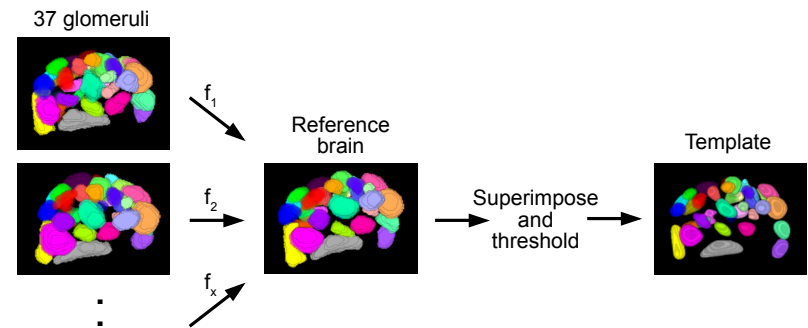
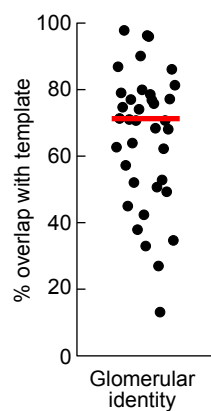
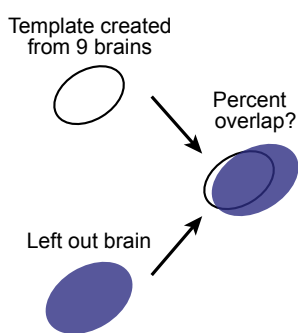
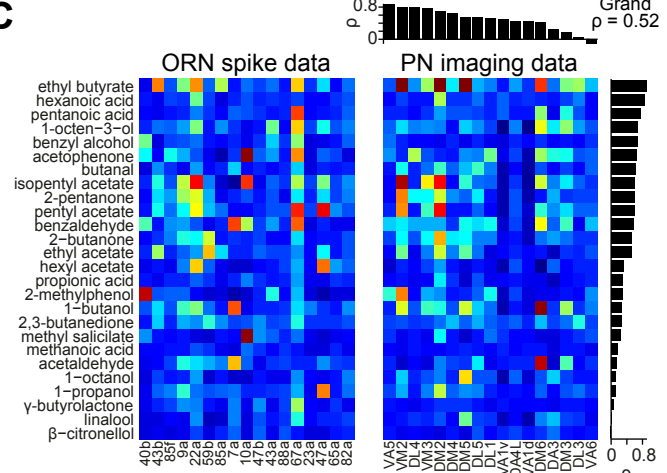
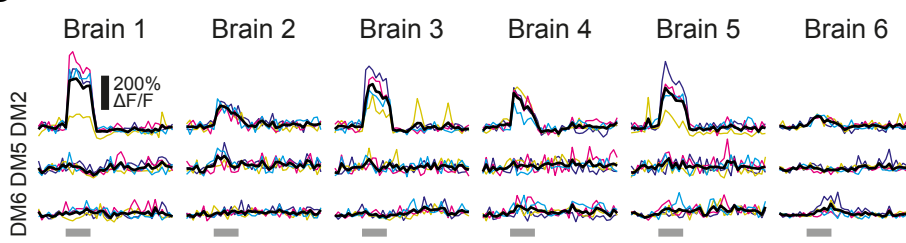
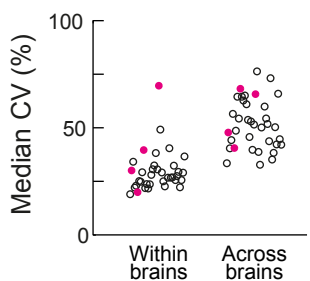
**B****C****D****E**

Figure S3 (related to Figure 2). Characterization of the accuracy of the image registration procedure

(A) Creation of the template brain used for registering 2-photon images. (1) Individual brains are stained with antibodies to reveal the morphology of glomeruli (nc82) and transgene expression (anti-GFP, not shown), and imaged at high resolution. The brain was scanned with dorsal side up. Shown are 4 representative slices separated by 18 μm . Scale bar, 20 μm . (2) 37 *NP255-Gal4*-positive glomeruli are manually delineated based on nc82 and anti-GFP signals. (3) Delineated glomeruli in each brain are registered to a reference brain by computing the affine transformation which maximizes the cross-correlation between 4 guidepost glomeruli (DL3, DA2, VM2 and DM5). (4) The 37 delineated glomeruli in all registered brains are superimposed, and thresholded to obtain a template that covers 50% of the mean volume of each glomerulus.

(B) The quality of the registration procedure is assessed by computing, for each glomerulus, the overlap between its volume in individual registered brains and the template. This comparison was repeated 10 times, each time leaving out a different brain. The average overlap over the 10 left-out brains is reported for each glomerulus. The median overlap (red bar), computed across all glomeruli, was 70.8%.

(C) Comparison of PN responses in our data set with the ORN data of Hallem and Carlson (2006), including odors and glomeruli/ORNs that are common to both data sets (arbitrary color scale with warmer colors indicating stronger responses). Bar graphs show the Pearson correlation between both data sets, for each glomerulus and each odor. The Pearson correlation between the entire data sets was 0.52.

(D) Example $\Delta F/F$ traces in response to hexanoic acid in 3 neighboring glomeruli (DM2, DM5 and DM6), for 4 trials of odor application (colored lines), and across all measured brains ($n = 6$). The thick black line denotes the average over 4 trials; the gray bar indicates the period of odor application. The response of DM2 is consistently observed across trials and brains, and no contamination is seen in the other 2 glomeruli, which are not activated by hexanoic acid.

(E) The variability of glomerular responses is summarized using the coefficient of variation (CV). Within-brain variability is assessed by computing, for each glomerulus, the CV of the 4 response trials and taking the median of this quantity across odors and brains. Across-brain variability is assessed by computing trial-averaged responses for each glomerulus, computing their CV across all measured brains and taking the median of this quantity across odors. In both cases, the computation is restricted to odors for which the glomerulus exhibited significant responses. Magenta dots correspond to guidepost glomeruli.

These data suggest that our registration procedure reliably extracts individual glomerular responses without substantial contamination from neighboring glomeruli. We cannot, however, rule out some degree of contamination due to animal-to-animal variability in AL morphology, the extent of which is assessed by the analysis in B. Nevertheless, because morphological variation must occur randomly, it can be safely assumed that no systematic contamination is present in our data. Furthermore, the impact of randomly-occurring contamination can be expected to be minimized after averaging over many brains. To assess the potential impact of such contamination on the result of our analyses more directly, we performed numerical simulations in which contamination was artificially introduced in every glomerulus of every brain by mixing its response with 10% or 20% of the response of one of its 3 nearest neighbors (for each glomerulus, one neighbor was picked at random in each brain). We then repeated our entire analysis and assessed the impact of the contamination on the results. We found that the impact was minimal; in particular, glomerulus weights were always very highly correlated with the original weights of Figure 4.

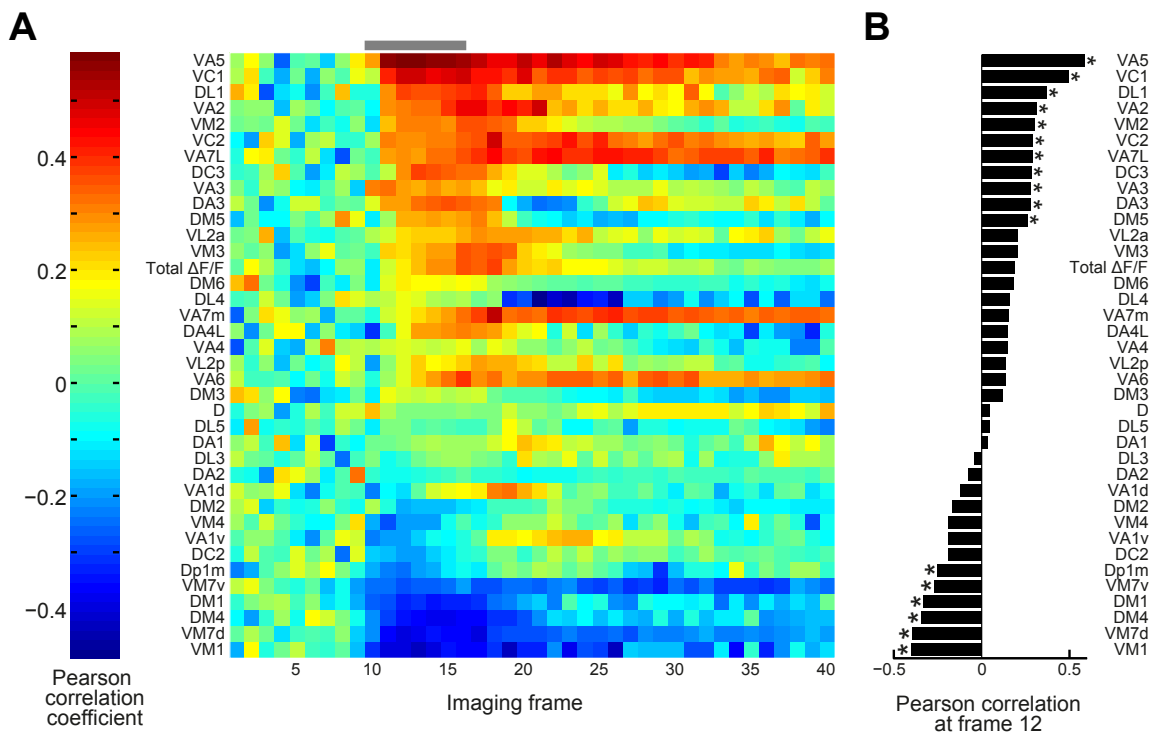


Figure S4 (related to Figure 2). Linear correlations between PN and behavioral responses

(A) Pearson correlation coefficient between PN $\Delta F/F$ activity and VI values, calculated over a data set of pure odors and mixtures (72 odors). Data is color-coded according to the scale bar on the left. Glomeruli are arranged by increasing correlation. The gray bar at the top indicates the period of odor application.

(B) Histogram of the Pearson correlation coefficient at imaging frame 12. Asterisks indicate significant values at the $p < 0.05$ level. Glomeruli are arranged in the same order as in A. The total $\Delta F/F$ (sum of $\Delta F/F$ over all 37 glomeruli) is positively, but weakly correlated with VI, indicating that odor valence is not solely dependent on the overall intensity of PN activation. Note that the rank-order of glomeruli differs from the regression result of Figure 4, as the correlation measures the strength of the linear relationship between a glomerulus' activity and the VI without considering the influence of other glomeruli. In some cases (e.g., VA2, VC1, Dp1m), the apparent sign of the relationship indicated by the correlation may also reverse when other predictors are taken into account.

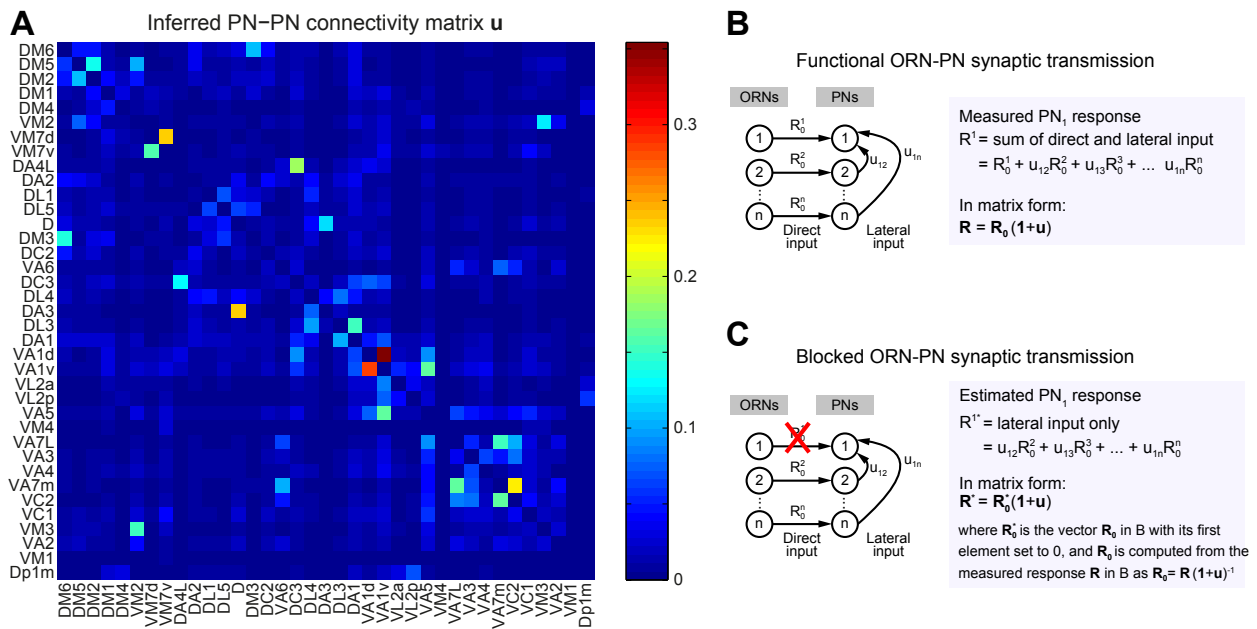


Figure S5 (related to Figure 5). PN-PN connectivity inferred from Ca^{2+} imaging data

(A) Inferred connectivity matrix between 37 glomeruli. The strength of connections is color-coded according to the scale bar on the right.

(B) Model assumed in estimating the connectivity matrix. PNs in each glomerulus receive, in addition to direct ORN input, lateral input from all the other glomeruli, which scales with the strength of their connection. The observed total PN activity is thus the sum of the activity evoked by direct input \mathbf{R}_0 and lateral input $\mathbf{R}_0\mathbf{u}$ where \mathbf{u} denotes the connectivity matrix in A.

(C) Calculation used to estimate PN activity in the case where ORN-PN synaptic transmission is blocked in specific glomeruli. The activity due to direct ORN input, \mathbf{R}_0 , is first calculated from the observed data \mathbf{R} by inverting the relation in B. The elements of \mathbf{R}_0 corresponding to the blocked glomeruli are then manually set to zero, and this is re-convolved with the connectivity matrix to obtain the estimated activity \mathbf{R}^* .

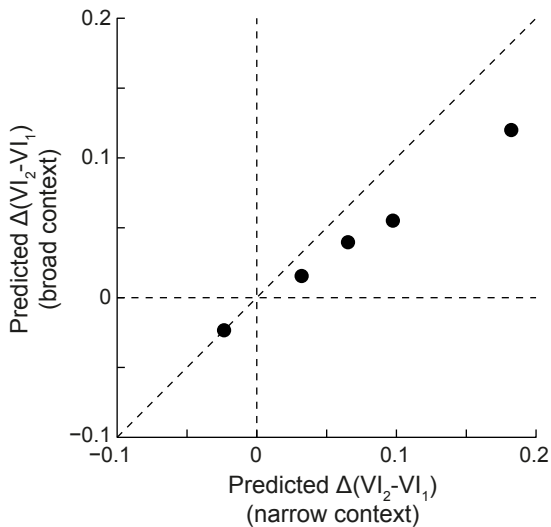


Figure S6 (related to Figure 7). Comparison of model predictions for the change in relative valence as a function of the breadth of the olfactory context

The graph shows theoretical predictions relating to the experimental data for the “same flies” condition of Figure 7E. Flies are presented with a set of 6 odors (context A) in the first half of the experiment, and a different set of 6 odors (context B) in the second half. The relative valence of odor pairs in the first half is computed relative to context A. For the second half, however, it may be computed either relative to context B only (“narrow context”), or, assuming that flies are still affected by the presentation of the previous context, relative to the sum of contexts A and B (“broad” context), leading to different predictions.

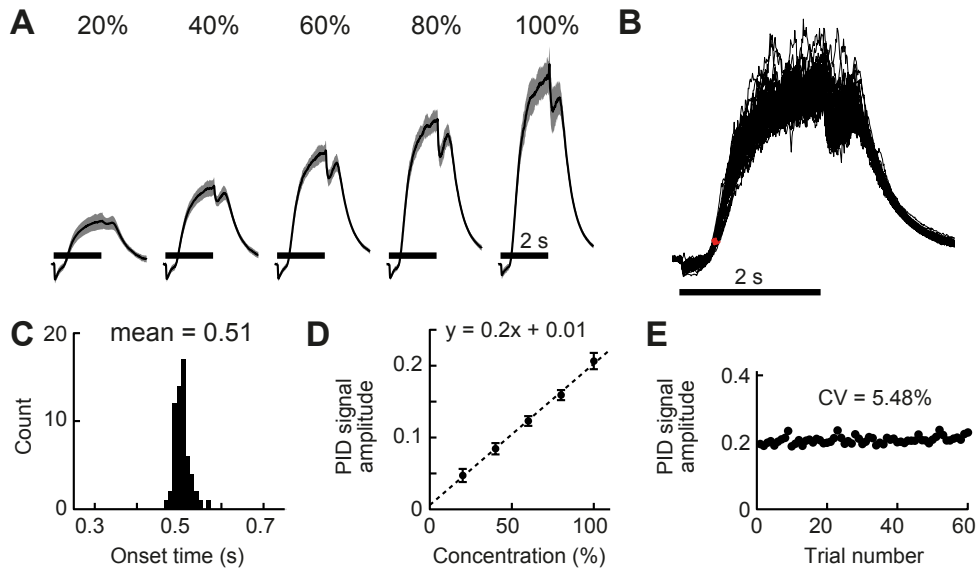


Figure S7 (related to Experimental Procedures). Characterization of the odor delivery system

(A) Average photo-ionization detector (PID) signal time course in response to 4-methyl-cyclohexanol (MCH) mixed with mineral oil at various ratios. Odor is delivered by bubbling the air stream through various combinations of 5 MCH (50% dilution) and 5 mineral oil vials. Labels indicate the ratio of MCH-to-oil vials. Scale bar denotes the period during which solenoid valves were open. Gray shade indicates SEM.

(B) Individual traces corresponding to the 100% condition in A. Overlaid are 60 traces obtained by opening between 1 and 5 MCH-loaded channels, showing that (i) the signal is stable across repetitions, and (ii) the number of open channels does not affect odor delivery significantly. Odor onset times (10% rise time) are shown in red.

(C) Histogram of odor onset time (10% rise time of PID signal, red dots in B) for the 100% condition, showing little variability around its average (0.51 s).

(D) Response amplitude (average PID signal in 1.5-2 s after solenoid valve opening) plotted against the concentration of MCH (ratio of MCH-to-mineral oil vials), showing a linear increase. Dashed line: linear fit. Error bars indicate the standard deviation.

(E) Response amplitude as a function of repeat number for the 100% condition, showing stability across repeats (each MCH-carrying channel was opened between 237 and 276 times across the duration of the experiment).

Pure odors (36 odors)

odor	rank in Fig 1F	solvent	dilution	vendor	odor sets
1-octanol	34	oil	10 ⁻²	Sigma-Aldrich	P ₁ ,T ₂ ,X ₁
3-octanol	32	oil	10 ⁻²	Tokyo chemical industry	P ₂
4-methylcyclohexanol	31	oil	10 ⁻²	Sigma-Aldrich	P ₂
geosmin	19	oil	10 ⁻²	Sigma-Aldrich	P ₄
1-octen-3-ol	13	oil	10 ⁻²	Tokyo chemical industry	P ₅ ,T ₃
1-butanol	17	water	10 ⁻²	nacalai tesque	P ₅ ,T ₂ ,X ₁ ,X ₂
methanoic acid (formic acid)	26	water	10 ⁻²	Sigma-Aldrich	P ₁ ,X ₁ ,X ₂
hexanoic acid	30	water	10 ⁻²	Sigma-Aldrich	P ₁
pentanoic acid (Valeric acid)	28	water	10 ⁻²	Sigma-Aldrich	P ₂
2-oxopentanoic acid	14	water	10 ⁻²	Sigma-Aldrich	P ₃ ,X ₁
propionic acid	7	water	10 ⁻²	Wako	P ₄
ethyl butyrate	20	oil	10 ⁻²	Sigma-Aldrich	P ₂ ,T ₂ ,T ₃
hexyl acetate	33	oil	10 ⁻²	Wako	P ₃
isopentyl acetate	12	oil	10 ⁻²	Wako	P ₃ ,T ₂ ,X ₂
ethyl acetate	11	oil	10 ⁻²	Sigma-Aldrich	P ₄ ,T ₂ ,X ₂
pentyl acetate	4	oil	10 ⁻²	Sigma-Aldrich	P ₅
benzaldehyde	37	oil	10 ⁻²	Sigma-Aldrich	P ₂ ,T ₁
2-methylphenol (o-cresol)	38	oil	10 ⁻²	Sigma-Aldrich	P ₂ ,T ₁
acetophenone	35	oil	10 ⁻²	Sigma-Aldrich	P ₁ ,X ₁
benzyl alcohol	15	water	10 ⁻²	Wako	P ₄ ,X ₁
methyl salicylate	8	oil	10 ⁻²	Sigma-Aldrich	P ₅
2,3-butanedione (Diacetyl)	9	water	10 ⁻²	nacalai tesque	P ₂
2-pentanone	1	oil	10 ⁻²	Wako	P ₃ ,T ₃
2-butanone	3	water	10 ⁻²	Sigma-Aldrich	P ₅ ,T ₃ ,X ₂
butanal (butyraldehyde)	36	oil	10 ⁻²	nacalai tesque	P ₂ ,T ₁
acetaldehyde	29	water	10 ⁻²	Wako	P ₃
β -citronellol	16	oil	10 ⁻²	Wako	P ₄
linalool	23	oil	10 ⁻²	nacalai tesque	P ₄ ,T ₂
γ -butyrolactone	24	water	10 ⁻²	Sigma-Aldrich	P ₁
3-methylthio-1-propanol	27	water	10 ⁻²	Sigma-Aldrich	P ₂ ,X ₂
phenylethylamine	25	water	10 ⁻²	Wako	P ₃
apple cider vinegar	5	NA	1	Mizkan	P ₂ ,T ₁
mango mimic ^a	18	water	10 ⁻²	see Other components	P ₂ ,T ₁ ,T ₃
broth	6	water	10 ⁻²	Yamasa	P ₂ ,T ₁
vinegar mimic ^b	22	water	10 ⁻²	see Other components	P ₁ ,T ₃
banana essence	2	water	10 ⁻²	Narizuka corporation	P ₅

Mixtures (3 x 3 = 9 mixture sets, 36 different mixtures excluding pure components)

odor A	odor sets	odor B	odor sets
apple cider vinegar	M ₁ ,M ₂ ,M ₃	benzaldehyde	M ₁ ,M ₄ ,M ₇
mango mimic	M ₄ ,M ₅ ,M ₆	2-methylphenol	M ₂ ,M ₅ ,M ₈
broth	M ₇ ,M ₈ ,M ₉	butanal	M ₃ ,M ₆ ,M ₉

odor A:odor B = 100:0, 80:20, 60:40, 40:60, 20:80, 0:100

Concentration series (12 odors, excluding the concentration used in the pure odor set)

odor	solvent	dilution	steps	odor sets
apple cider vinegar	water	10 ⁻¹ ~ 10 ⁻³	10 ⁻¹	C ₁
mango	water	10 ⁻³ ~ 10 ⁻⁵	10 ⁻¹	C ₂
benzaldehyde	oil	10 ⁻³ ~ 10 ⁻⁵	10 ⁻¹	C ₁
2-methylphenol	oil	10 ⁻³ ~ 10 ⁻⁵	10 ⁻¹	C ₂

Other components (for mango mimic and vinegar mimic)

odor	vendor
ethanol	Junsei chemical
acetic acid	Wako
2-phenylethanol	Wako
ethyl acetate	Sigma-Aldrich
acetoin	Sigma-Aldrich

a. Ethanol, acetic acid, and 2-phenyl ethanol were mixed at a ratio of 1:22:5 (volume) as described in Zhu et al. (2003).

b. We modified the composition described in Becher et al. (2010) by taking vapor pressure and density into account, and dissolved acetic acid, 2-phenyl ethanol, acetoin, and ethyl acetate in ethanol at a ratio of 1:13.48:0.21:0.012 (volume).

Table S1 (related to Figure 1). List of odors used in the study

The table lists the 84 odors used in the study. Odor sets are divided into 5 categories: pure odors (P), mixtures (M), concentration (C), TNT (T) and context (X).

Table S2 (related to Figure 2). Mean Ca²⁺ responses of PNs in 37 glomeruli to a set of 84 odors

The table gives the mean PN activity ($\Delta F/F$ averaged over odor application period, frames 10-17) in 37 glomeruli in response to the 84 odors used in the study, including the 36 odors displayed in Figure 2.

Figure	Genotype
1,2B-2E,3,7,S1,S3,S4,S6	<i>NP225-Gal4,UAS-IVS-GCaMP6f(attP40)/UAS-IVS-GCaMP6f(attP40)</i>
2A	<i>NP225-Gal4/UAS-mCD8::GFP</i>
5A,5D-5G	Blockade of single glomerulus: <i>F1 of Or-Gal4 x UAS-TNT-E2</i> <i>Or33c-Gal4</i> <i>Or42b-Gal4</i> <i>Or59b-Gal4</i> <i>Or83c-Gal4</i> <i>Or85a-Gal4</i> <i>Or85d-Gal4</i> <i>Or92a-Gal4</i> <i>UAS-TNT-E2/+ (control)</i>
	Blockade of three glomeruli: <i>Or85a-Gal4/UAS-TNT-E2;Or33c-Gal4/Or83c-Gal4</i> <i>Or85d-Gal4/UAS-TNT-E2;Or59b-Gal4/Or92a-Gal4</i>
5B,5C	<i>Or42b-Gal4/UAS-TNT-E2;GH146-QF[#53], QUAS-GCaMP3/QUAS-GCaMP3</i> <i>Or85a-Gal4/UAS-TNT-E2;GH146-QF[#53], QUAS-GCaMP3/GH146-QF[#53]</i>
6	<i>UAS-IVS-CsChrimson.mVenus(attP40);Or59b-Gal4</i>
S2	<i>Orco-Gal4/UAS-TNT-E2</i> <i>UAS-TNT-E2/+ (control)</i>

Genotype	RRID
<i>NP225-Gal4</i>	DGGR_112095
<i>Or33c-Gal4</i>	BDSC_9966
<i>Or42b-Gal4</i>	BDSC_9971
<i>Or59b-Gal4</i>	BDSC_22898
<i>Or83c-Gal4</i>	BDSC_23132
<i>Or85a-Gal4</i>	BDSC_23133
<i>Or85d-Gal4</i>	BDSC_24148
<i>Or92a-Gal4</i>	BDSC_23140
<i>Orco-Gal4</i>	BDSC_26818
<i>UAS-IVS-GCaMP6f(attP40)</i>	BDSC_42747
<i>UAS-IVS-mCD8::GFP(attP40)</i>	BDSC_32186
<i>UAS-TNT-E2</i>	BDSC_28837
<i>UAS-IVS-CsChrimson.mVenus(attP40)</i>	BDSC_55135
<i>GH146-QF[#53]</i>	BDSC_30015
<i>QUAS-GCaMP3</i>	BDSC_52231

Table S3 (related to Experimental Procedures). List of genotypes used in the study and associated RRIDs

All the flies are from the Bloomington Stock Center except for the following stocks: Michael Dickinson Laboratory wild type and *w[1118]* are gifts from Rachel Wilson; *NP225-Gal4* is a gift from Hiromu Tanimoto; *GH146-QF[#53]* is a gift from Christopher Potter.

Movie S1 (related to Figure 1). Reconstruction of a behavioral trial exemplifying aversive and attractive responses

The movie shows a sequence of snapshots taken using the infrared camera along with a reconstruction of the visual stimulus delivered to the fly during the trial. An aversive odor (benzaldehyde) is delivered at $t = 6.5$ s, and an attractive odor (apple cider vinegar) at $t = 16.5$ s.

Movie S2 (related to Figure 2). Representative odor response of PNs

Representative response to 3-octanol in *NP225-Gal4* positive PNs expressing GCaMP6f imaged with two-photon microscopy. Thirty different focal planes aligned from top-left to bottom-right along the dorsoventral axis are separated by 3 μm . $\Delta F/F$ signal (pseudo-color, average of four trials) is overlaid on the structure of the AL (grayscale). A white bar indicates the 4 s odor application period and measures 10 μm . The movie is sped up 6 times.

SUPPLEMENTAL EXPERIMENTAL PROCEDURES

Fly Stocks

Flies were raised on conventional cornmeal agar medium under a 12 hr light/ 12 hr dark cycle at 25 °C. The density of culture was controlled to be sparse. All experiments were performed on adult female flies, 2-4 days after eclosion. Therefore, our results technically do not apply to males. Flies were starved for 4-6 h with water prior to experiments. The following stocks were used: Michael Dickinson Laboratory wild type ([Bhandawat et al., 2010](#)), *UAS-GCaMP6f(attP40)* ([Chen et al., 2013](#)), *UAS-TNT-E2* ([Sweeney et al., 1995](#)), *UAS-mCD8::GFP*, *NP225-Gal4* ([Tanaka et al., 2012; Thum et al., 2007](#)), *GH146-QF* ([Potter et al., 2010](#)), *QUAS-GCaMP3* ([Tian et al., 2009](#)), *UAS-Chrimson* ([Klapoetke et al., 2014](#)), and *Or-Gal4* lines ([Couto et al., 2005](#); [Fishilevich and Vosshall, 2005](#); [Larsson et al., 2004](#)) including *Or33c-Gal4*, *Or42b-Gal4*, *Or59b-Gal4*, *Or83b-Gal4* (*Orco-Gal4*), *Or83c-Gal4*, *Or85a-Gal4*, *Or85d-Gal4*, *Or92a-Gal4*. For Chrimson experiments, 200 mM all-transretinal dissolved in ethanol was mixed with fly food and fed to the flies for 3 days prior to experiments. All stocks were back-crossed 6 generations to Dickinson Laboratory wild type flies carrying *w¹¹¹⁸* except for Q system flies. Detailed genotypes of flies used in each experiment are listed in Table S3.

Olfactory Stimulation

Odors were delivered by passing an air stream through 4 ml of odorant solution (using either mineral oil or water as a solvent) in a glass vial. The air stream (250 ml/min) was split into 16 parallel channels each lined up with a single odor vial and a solenoid valve (100E1-SR, Koganei Corporation) that regulated the open/closed state of the channel. The outputs of all channels were pooled, mixed into the main air stream (1.55 l/min), and directed into the behavioral chamber using ø6 mm Teflon tubing (main tube). A small portion of this air stream was diverted from the main tube through a ø2 mm outlet tube and delivered frontally to the fly. This configuration reduced the impact of transient changes in air pressure caused by the switching of solenoid valves, and was critical not to disturb flight at the onset of odor delivery. The tip of the delivery outlet was placed 10 mm away from the fly. The remainder of the air stream, which was not delivered to the fly, was directed out of the chamber and cleared using a fume hood fan unit (3-4064-11, AS ONE). Because the quantity of air reaching the fly decreased with increasing suction of the fan unit, suction power was calibrated to obtain an air flow of 0.3 m/s at the fly location, using an air flow sensor (QB-5, Tohnic). Odors delivered inside the chamber were actively removed by a suction tube placed behind the fly. Binary mixtures of two odors A and B were obtained by simultaneously circulating air through 5 channels, each loaded with either A or B, and varying the relative number of A and B channels. This method was chosen because the concentration of delivered odor, as measured using a photo-ionization detector (200B miniPID, Aurora Scientific Inc.), varied linearly (Figure S7). To avoid odor contamination, Teflon was used for all parts that came in contact with odorized air, and tubing was periodically washed with alcohol, rinsed with purified water, and dried with clean air. A total of 84 odors were used in the study (Table S1).

Behavioral Experiments

Flies were cold-anesthetized on a Peltier device and tethered to a stainless steel pin (Austerlitz minutiens ø0.1 mm) between the head and thorax, using ultraviolet-curing adhesive (NOA 63, Norland). Tethered flies were placed in a glass vial equipped with a piece of filter paper soaked with purified water to prevent dehydration, starved, and transferred to the flight-simulator arena. The setup consisted of an odor delivery apparatus and a 24x56 array of green LEDs ([Reiser and Dickinson, 2008](#)) arranged in a half circle (Mettrix Technology Corp.). The display spanned ~210 deg horizontally, and ~56 deg vertically below the fly. The entire setup was enclosed in an opaque container to prevent light entry, and the tethered fly was illuminated with infrared LEDs to allow visualization using a camera (Lu070M, Lumenera corporation).

Flight behavior was monitored using two microphones (AT9904 electret condenser microphones, audio-technica) positioned laterally ~1 mm from the tip of the extended wing on either side of the fly, whose outputs were amplified (AT-MA2 amplifier, audio-technica), digitized (NI 9215, National Instruments) and analyzed in real-time using a desktop computer (Optiplex 980, Dell) to extract the turning direction and speed, which were used to update the visual and olfactory stimuli in closed-loop. The visual stimulus was essential to increase flight reliability, and consisted of vertical gratings with a spatial frequency of 60 deg⁻¹. The panel of 84 olfactory stimuli was divided in sets of 6 odors (Table S1) and a single set was applied in each experiment (except for the data in Figure 7E, “same flies” condition, where two sets were applied consecutively). The protocol consisted of 15 blocks, in which each of the 6 odors, as well as a control odor (mineral oil), were applied in randomized order, up to a fixed duration (4 s unless otherwise stated) and in a restricted spatial region (45 deg centered at the fly location at the time of odor contact). Odor application was terminated when the fly exited this spatial region, but was re-initiated if the fly re-entered the region within the application period. For optogenetic activation experiments, a 637 nm laser (HL63142DG, Thorlabs) was positioned in the setup and controlled in closed-loop in the same way as odorant stimuli. Before each experiment, the laser was adjusted to target the antennal region. Inter-trial-interval was 10 s unless otherwise stated. When no odor was applied (including inter-trial intervals), air was presented in order to maintain a fixed air flow. The random sequence of odor presentation was fixed across experiments and chosen not to present the same odor consecutively at the transition between successive blocks. After post-hoc data analysis, data from individual flies were used for analysis if the flying percentage during the entire experiment exceeded 50% (resulting in a rejection rate of ~1/10). For each data set, experiments were conducted until data were collected from 20 flies. This number was chosen on the basis of preliminary experiments to obtain a sufficient signal-to-noise ratio.

Closed-loop control of the visual display and solenoid valves was achieved using a data-acquisition board and modules (NI cDAQ9178, NI 9215, NI 9264, National Instruments) and custom software written in Matlab (Mathworks), Java and C. Briefly, microphone signals were acquired continuously in chunks of 5 ms, and signal amplitude in each chunk was computed as the difference between the maximum and the minimum values. These amplitudes were filtered by calculating the median over the 3 most recent values and (i) summed to obtain the flight strength s , and (ii) standardized (using mean and standard deviation values computed over the previous block of trials; for the first block, running estimates computed before the experiment were used) to obtain the standard left and right wing-beat amplitudes w_L and w_R . Turns during flight were assessed by monitoring the difference in wing-beat amplitudes, a proxy for yaw torque (Tammero et al., 2004). An increment $\Delta\theta$ in angular position was registered if the difference in standard wing-beat amplitudes $\Delta w = w_R - w_L$, after multiplication by the flying strength, exceeded the value of its standard deviation $\sigma_{\Delta w}$ (computed over the previous block of trials), above which the increment was proportional to Δw , i.e., $\Delta\theta = \gamma \text{sign}(\Delta w) \max(0, |\Delta w|s - \sigma_{\Delta w})$, with a coupling coefficient $\gamma = 0.375$ to yield units of degrees. Angular position was computed by cumulatively summing these increments, and odorant and visual stimuli were updated every 5 ms in accordance with the current position. The validity of computing the turning propensity from microphone data was verified by comparing with the wing angles obtained from video data; the two methods yielded highly similar results (Figure S1).

A total of 84 odors were tested with the set repartition listed in Table S1. The analysis in Figures 4B-4D was conducted using 5 pure odor sets P₁-P₅ and 9 mixture sets M₁-M₉. The final model was thus estimated using these 14 sets but none of the other data. For Figure 4E, two additional test sets, concentration sets C₁-C₂, were used. For these sets, odors evoking strong behavioral responses were chosen because of the expectation that lowering the concentration would reduce the amplitude of the responses. For Figure 5, single-ORN experiments were all conducted using the same odor set, T₁, with the exception of DM5 which was additionally tested with T₂. Triple-ORN experiments were conducted using sets T₂ (DM5+DC3+VC1) and T₃ (DM4+VA2+VA4). For Figure 7D, additional experiments were conducted using sets X₁ and X₂, and results were pooled with previous experiments using sets P₁ and P₅ to compare relative valences. For Figure 7E, “same flies” condition, experiments were

conducted by presenting sequentially X₁ and X₂, X₁ and P₁, or X₂ and P₅, with the exact same protocol as in other experiments except that odors were changed after the 8th block.

Two-photon Imaging

Individual starved flies were attached to a custom recording plate modified from Maimon et al. (2010) with ultraviolet-curing adhesive (NOA 63, Norland) while cold-anesthetized. Flies were attached at their anterodorsal end of the thorax, posterodorsal end of the head, and dorsal edges of the compound eyes. A small hole was made on the plate to access the head cuticle for dissection, with most of the fly body remaining below the plate. The plate was designed using computer-aided design software (Rhinoceros 5.0, Robert McNeil and Associates) and milled out of Delrin plastic with an MDX-540SA milling machine (Roland DG) controlled by computer-aided manufacturing software (Craft MILL, C & G Systems). After attaching the flies, saline bubbled with 95% O₂/5% CO₂ was added on the plate, and the head cuticle was removed with forceps to expose the brain of *NP225-Gal4,UAS-GCaMP6f/UAS-GCaMP6f* flies. Saline contained (in mM): 103 NaCl, 3 KCl, 5 N-tris(hydroxymethyl) methyl-2-aminoethane-sulfonic acid, 8 trehalose, 10 glucose, 26 NaHCO₃, 1 NaH₂PO₄, 1.5 CaCl₂, and 4 MgCl₂ (osmolarity adjusted to 270–275 mOsm). Saline was perfused at a rate of 2 ml/min during the recording. The muscle of the frontal pulsatile organ (number 16) was severed to alleviate brain movement.

The entire right AL was imaged with a two-photon laser scanning microscope (LSM 710 NLO, Zeiss) equipped with a water immersion objective lens (W Plan-Apochromat, 20x, numerical aperture 1.0). The fluorophore was excited with a titanium:sapphire pulsed laser (Chameleon Vision II, Coherent) mode-locked at 930 nm. Laser power was set between 3–6 mW at the back aperture of the objective lens. Fluorescence was collected with an internal GaAsP detector through a bandpass emission filter (BP470-550). A piezo positioner (P-725.2CD PIFOC, PI) moved the objective lens vertically, allowing the system to cover 33 optical slices separated by 3 μm in 595 ms (18 ms/slice). Such three-dimensional (3D) images of the AL were acquired repetitively during functional imaging, corresponding to volume scanning at a rate of ~1.7 Hz. After applying digital zoom, the pixel size in a slice was 1.384 x 1.384 μm, which was sufficient to resolve individual glomeruli measuring on average ~10 μm in diameter.

The odor delivery system was identical to that used in behavioral experiments, and the properties of both systems were scrupulously matched. In each experiment, an odor set consisting of 15 pure odors or 6 odor mixtures was applied. Each odor in the set was presented for 4 s, with an inter-trial-interval of 1 min between odors. Odor valves opened in frame 9 and closed in frame 16. Each set was presented 4 times, and the order of odor presentation was randomized in each block. The sequence of odor presentation was fixed across experiments of the same type and chosen not to present the same odor consecutively at the transition between two successive blocks. After collecting odor responses, 1 μM tetrodotoxin was added to the saline and a high-resolution 3D image of the AL comprising 99 optical slices (1 μm interval, 0.346 x 0.346 μm pixel size) was acquired for off-line identification of guide-post glomeruli (see Data Analysis section).

Immunohistochemistry and Structural Imaging

Brains were dissected out from the head capsule in phosphate-buffered saline (PBS) and fixed with 4% paraformaldehyde in PBS for 90 min on ice. Each brain was washed 3 times over an hour and incubated in blocking solution containing 5% normal goat serum in PBST (0.2% Triton-X in PBS) for 30 min. Primary antibodies were added and incubated at 4 °C for ~48 hr. After removal of antibodies and washing over an hour, the brain was incubated in a solution of secondary antibodies at 4 °C for 24 hr. The brain was then washed, immersed in PBS, and positioned with its dorsal side up on a MAS-coated glass slide (Matsunami). Images were collected with an LSM 710 NLO confocal microscope (Zeiss) using a water immersion lens. The only exception was the brain in Figure 2A, which was immersed in Vectashield (Vector laboratories), positioned anterior side up on a glass slide, sealed with a cover glass, and imaged with a FV1000 confocal microscope (Olympus) using an oil immersion lens. The following

antibodies were used at the indicated dilution: mouse nc82 (1:20, Developmental Studies Hybridoma Bank at Univ. of Iowa, RRID: AB_528108), rat anti-GFP (1:1000, nacalai tesque, RRID: AB_10013361), anti-mouse CF633 (1:250, Biotium, RRID: AB_10556971), and anti-rat CF488 (1:250, Biotium, RRID: AB_10557403).

ORN Recordings

ORN recordings were performed as previously described ([Kazama and Wilson, 2009](#)). Ab2 sensilla were identified on the basis of morphology, number of distinct spikes and response to ethyl acetate.

Data Analysis

Data were analyzed with custom codes written in Matlab (Mathworks) unless otherwise stated.

Behavioral data analysis. Valence indices (VIs) for individual flies were obtained by aligning flight trajectories to the time of odor contact (0.5 s after odor valve opening, see Figure S7) and calculating the proportion of time spent outside the odor plume for each odor. The instantaneous VI was calculated in every 5 ms time bin, and the mean VI (simply referred to as VI throughout the text) was calculated as an average over the last 1 s of odor presentation period. The mean and standard error were then computed by pooling all tested flies. ΔWBA in Figure 1G was calculated using the absolute difference in the standardized wing-beat amplitudes (c.f. Behavioral Experiments section) and averaged in 100 ms bins before pooling over tested flies. Trials in which flight was interrupted were excluded from the analysis.

Two-photon imaging data analysis. To quantify PN odor responses in individual glomeruli, images were analyzed in three steps: correction for brain motion, creation of template glomeruli, and extraction of fluorescence changes in each glomerulus using the template.

To correct for brain motion, each 3D image resulting from a full AL scan was re-aligned to the high-resolution 3D image with sub-pixel precision. Re-alignment was achieved by shifting the target image in a Cartesian coordinate system so as to maximize the cross-correlation between the two images.

To extract fluorescence changes in individual glomeruli in an efficient and objective manner, we constructed a template AL against which all images were registered. To obtain the template, 37 *NP225-Gal4*-positive glomeruli were delineated in immunostained brains based on nc82 and anti-GFP signals using the Fiji ([Schindelin et al., 2012](#)) segmentation editor (Figure S3). Delineated glomeruli in different brains were registered to the reference brain by optimizing an affine transformation to maximize the cross-correlation between four guidepost glomeruli (DL3, DA2, VM2, and DM5), and applying this transformation to the whole brain (Figure S3). These particular glomeruli were selected as guideposts because they are strongly labeled by *NP225-Gal4*, jointly cover a wide surface of the AL, and because four is the minimal number of points required to determine a rigid body. A larger number of guidepost glomeruli were not used because they would collectively resemble a sphere, in which case the cross-correlation between the two images may exhibit several maxima. Registered glomeruli were superimposed and thresholded to obtain the template AL, in such a way that each glomerulus in the template covers 50% of the mean volume of the corresponding glomerulus. This moderate threshold volume was chosen to increase the probability that template glomeruli fall within the boundaries of actual glomeruli. Using this procedure, the median overlap computed across glomeruli was 70.8% with respect to the template volume (Figure S3).

At the end of each experiment, images were registered to the template AL by first delineating the four guidepost glomeruli using the high-resolution image (see Two-photon imaging section). The affine transformation maximizing the cross-correlation between the four glomeruli and the template was then computed and applied to all images. Data from individual brains was discarded without further analysis if the correlation with the template was lower than 0.6 in the 4 guidepost glomeruli. Finally, the template volume was used to calculate the relative change in fluorescence $\Delta F/F = (F_t - F_{\text{baseline}})/F_{\text{baseline}}$ in each glomerulus. Table S2 summarizes the mean response of each of the 37 glomeruli to the 84 odors in our data set. For the classification analysis of Figure 2E, an error-correcting output

codes (ECOC) multiclass model was trained using the fitcecoc.m function in Matlab. At each time frame, a classifier was trained using the responses of 37 glomeruli to 84 odors in 3 of the 4 imaging trials, and the data from the remaining trial was used to test classification performance.

Decoding analysis. Raw PN $\Delta F/F$ data were pre-processed as follows. For each imaging trial, a Mann-Whitney U-test ($p < 0.01$) was used to determine the glomeruli whose response (frames 12-15) differed significantly from the baseline (frames 2-8). Glomeruli that responded significantly and with the same mode (excitation or inhibition) in more than half of the trials were marked as responding, and their mean response was computed by averaging over the corresponding trials. For other glomeruli, the mean response was computed by averaging over non-significant trials. This procedure was employed because some glomeruli showed occasional failures in their responses; however, including all imaging trials had no qualitative impact on the result of our analyses.

For the normalization model, PN data was standardized in each glomerulus using mean and standard deviation values computed independently for each individual set of 6 odors, by pooling trial-averaged $\Delta F/F$ responses (imaging frames 12 to 16) over all 6 odors. Importantly, the statistics of glomerular activity are local quantities determined by the history of olfactory stimuli: because a different group of 6 odors was tested in each set of experiments, the same normalization parameters were used for odors in the same group, whereas different parameters were used for odors in different groups. VI values were similarly centered by subtracting their mean value over the 6 odors.

We fit the model using linear regression. Because of the large number of predictors, it was necessary to use a regularization procedure to avoid overfitting the training data. We used partial least-squares (PLS) regression, a technique known to be efficient in problems with many predictors and robust to collinearity in the predictors (Abdi, 2010). A number of regularization methods, including methods that favor sparse readout weights (e.g., LASSO), were also tested but consistently yielded poorer results. Briefly, the PLS method linearly transforms the set of predictor variables into a set of explanatory factors and regresses the dependent variable on the factors. The factors are calculated similarly as in principal component analysis, except that whereas principal component analysis finds directions of maximum variance in the predictors, PLS searches for directions of maximal covariance between the predictors and the dependent variable. Regularization is achieved by limiting the number of factors included in the regression, which can be achieved by cross-validating using a validation set. In our analysis, we used the following cross-validation procedure. In each validation round, one of the 9 binary mixture sets was taken as the test set, and was therefore excluded from the fitting procedure. The 4 other mixture sets that shared a common odor with the test set were also excluded from the fitting procedure to avoid training/test set contamination. The remaining 4 mixture sets, which did not share a common odor with the test set, were used for validation. The training set comprised the 30 pure odors that did not appear in the mixtures. We computed the PLS factors by pooling the training and validation sets using the plsregress function in Matlab. We then regressed the VI values on the factors using the training data only, by means of the fitlm function, and evaluated the performance of the resulting model on the validation set by calculating the R^2 coefficient. The optimal number of factors was chosen to maximize the validation R^2 . This resulted in 2-8 retained factors (average 3.2), indicating that a significant amount of regularization was necessary.

After each validation round, predicted VI values for the test mixture (6 values) were computed using the fitted model. At the end of the 9 validation rounds, predicted values for the 9 mixture sets were pooled together (54 values), and prediction performance was assessed using the prediction R^2 , defined as $R^2 = 1 - E_{\text{pred}}^2 / \sigma^2$, where E_{pred}^2 is the mean-square prediction error calculated over the 9 mixture sets, and σ^2 is the variance of the test data. This coefficient was chosen because it provides a measure of the prediction error relative to the typical variation in the data, and is thus a quantitative measure of prediction performance that is directly comparable across multiple test sets. It should be noted that, unlike the conventional coefficient of determination (R^2 of fit), the prediction R^2 may

take negative values if the prediction error is larger than the typical variation in the data, which may happen, for example, if the predictions are shifted from the data by a constant offset.

The statistical significance of prediction R^2 values was assessed using a permutation test. 500 surrogate PN data sets were generated by randomly shuffling glomerular labels, and the entire decoding analysis was repeated for each set. Upper bounds on the p-values for the reported statistics were estimated from the distribution obtained with the surrogate data.

For the data of Figure 4C, the best subsets of each size were defined as those that performed best on the four data sets (training, validation, test and concentration) simultaneously. In practice, we selected the subset that maximized the quantity $\sum_i(r_i)^2 - \sum_{i>j}(r_i - r_j)^2$, where r_i denotes the R^2 coefficient for data set i , and indices i and j run over the 4 data sets.

For the analysis of TNT data, PN-PN connections were inferred from the noise correlation structure of Ca^{2+} signals in the period of baseline activity preceding odor application (imaging frames 1 to 8, Figure S5). PN responses \mathbf{R} were modeled using the equation $\mathbf{R} = \mathbf{R}_0(\mathbf{1} + \mathbf{u})$ where \mathbf{R}_0 represents the portion of PN activity due to direct ORN drive, $\mathbf{1}$ is the identity matrix, and \mathbf{u} is the PN-PN connectivity matrix. Given that ORNs fire independently in the absence of odorant stimulus (Kazama and Wilson, 2009), the connectivity matrix \mathbf{u} was calculated by jointly diagonalizing the covariance matrices of PN activities in the considered imaging frames, using a gradient descent algorithm.

SUPPLEMENTAL REFERENCES

- Abdi, H. (2010). Partial least squares regression and projection on latent structure regression (pls regression). WIREs Comp Stat 2, 97-106.
- Becher, P.G., Bengtsson, M., Hansson, B.S., and Witzgall, P. (2010). Flying the fly: Long-range flight behavior of *Drosophila melanogaster* to attractive odors. J Chem Ecol 36, 599-607.
- Larsson, M.C., Domingos, A.I., Jones, W.D., Chiappe, M.E., Amrein, H., and Vosshall, L.B. (2004). Or83b encodes a broadly expressed odorant receptor essential for *Drosophila* olfaction. Neuron 43, 703-714.
- Maimon, G., Straw, A.D., and Dickinson, M.H. (2010). Active flight increases the gain of visual motion processing in *Drosophila*. Nat Neurosci 13, 393-399.
- Reiser, M.B., and Dickinson, M.H. (2008). A modular display system for insect behavioral neuroscience. J Neurosci Methods 167, 127-139.
- Schindelin, J., Arganda-Carreras, I., Frise, E., Kaynig, V., Longair, M., Pietzsch, T., Preibisch, S., Rueden, C., Saalfeld, S., Schmid, B., *et al.* (2012). Fiji: An open-source platform for biological-image analysis. Nat Methods 9, 676-682.
- Tammero, L.F., Frye, M.A., and Dickinson, M.H. (2004). Spatial organization of visuomotor reflexes in *Drosophila*. J Exp Biol 207, 113-122.
- Zhu, J., Park, K.C., and Baker, T.C. (2003). Identification of odors from overripe mango that attract vinegar flies, *Drosophila melanogaster*. J Chem Ecol 29, 899-909.